Journal of the Atmospheric Sciences

# Evaluation of the assumptions in the steady-state tropical cyclone self-stratified outflow using three-dimensional convection-allowing simulations

--Manuscript Draft--

| | |
|---|---|
| **Manuscript Number:** | JAS-D-19-0033 |
| **Full Title:** | Evaluation of the assumptions in the steady-state tropical cyclone self-stratified outflow using three-dimensional convection-allowing simulations |
| **Article Type:** | Article |
| **Corresponding Author:** | Kerry Emanuel<br>Massachusetts Institute of Technology<br>Cambridge, MA UNITED STATES |
| **Corresponding Author's Institution:** | Massachusetts Institute of Technology |
| **First Author:** | Dandan Tao |
| **Order of Authors:** | Dandan Tao |
| | Kerry Emanuel |
| | Fuqing Zhang |
| | Richard Rotunno |
| | Michael Bell |
| | Robert Nystrom |
| **Abstract:** | The criteria and assumptions that were used to derive the steady-state tropical cyclone intensity and structure theory of Emanuel and Rotunno (2011) are assessed using three-dimensional convection-allowing simulations using the Weather Research and Forecasting model. One real-data case of Hurricane Patricia (2015) and two idealized simulations with and without vertical wind shear are examined. In all three simulations, the gradient wind balance is valid in the inner core region above the boundary layer. The angular momentum (M) and saturation entropy surfaces (s*) near the top of the boundary layer, in the outflow region and along the angular momentum surface that passes the low-level radius of maximum wind (MRMW) are nearly congruent, satisfying the criterion of slantwise moist neutrality in the vicinity of MRMW. The theoretically derived maximum wind magnitude above the boundary layer compares well with the simulated maximum tangential wind and gradient wind using the azimuthally averaged pressure field during the intensification and quasi-steady state of the simulated storms. The Richardson number analysis of the simulated storms shows that small Richardson number ($0<Ri \leq 1$) exists in the outflow region, related to both large local shear and small static stability. This criticality of the Richardson number indicates the existence of small-scale turbulence in the outflow region. We also show that the stratification of temperature along the M surface at the outflow region for steady-state hurricanes is approximately applicable in these 3-dimensional simulations, while the radial distribution of gradient wind is qualitatively comparable to the theoretical radial profiles. Some caveats regarding the theory are also discussed. |

**We thank all three reviewers for their specific, insightful and constructive comments, which are very helpful in our revision. We have made every effort to address all the concerns raised by the reviewers and revised our manuscript accordingly. Our point-by-point responses are given below.**

Reviewer #1

A Review of Evaluation of the assumptions in the steady-state tropical cyclone self-stratified outflow using three-dimensional convection-allowing simulations

By D. Tao, K. Emanuel, F. Zhang, R. Rotunno, M. Bell, R. Nystrom
Submitted to the Journal of Atmospheric Sciences

Recommendation: Major Revisions

**General Comments**

The authors evaluate the assumptions used as the basis for the steady-state tropical cyclone intensity and structure theory of Emanuel and Rotunno (2011) (ER11) and Emanuel and Rotunno (2012) (ER12). Two idealized simulations and one real data simulation of the extreme Hurricane Patricia are analyzed. The results of the author's analysis support the hypothesis of ER11 and ER12. I enjoyed reading this manuscript and I believe it may be an important research contribution that will be of great interest to the tropical cyclone community. The paper is well written, and in general, the figures are very clear. I particularly liked that the authors addressed each of the major assumptions in a concise manner. I have a few comments and suggestions related to the interpretation of the results that need to be addressed before the manuscript could be considered acceptable for publication. I also have a few questions regarding the model setup and the sensitivity of the results to some of the model parameters.

**General Comments**

1. I think the authors have done a very nice job laying out the key assumptions and systematically evaluating these based on the model simulations. After reading the paper, I did wonder 'how good is good enough' to sufficiently support the assumptions that the ER11/ER12 theory is based on. Could the authors show (or surmise) that the theory is insensitive to certain thresholds for each of the assumptions considered? In other words, it would be useful to state the threshold required for each assumption to be valid from a theoretical perspective. I think this will give more confidence in the evaluation of the validity of the criteria and assumptions used in the theory. This is done to some degree in Section 4, but not always in a very quantitative manner.
**Reply: The reviewer raised an intriguing question on whether there exists a quantitative threshold of each of the assumptions that were made to derive the theory. The focus of this study is to evaluate these assumptions in the three simulations but it is beyond the scope of the current study to give a theoretical perspective of the error bound in the ER11/ER12 theory beyond what is presented in Section 4.**

2. The theory is stated to be applicable for steady state situations and I wonder whether the Patricia case was really a good test for the assumptions evaluated in this manuscript. Patricia exhibited extreme intensification followed by rapid weakening. The time selected for evaluation is right at the peak intensity and it is clear from Fig. 1 that the intensity is not at a steady state. Some aspects of the Patricia simulations seemed to be an outlier relative to the two weaker and more steady state idealized simulations. More justification of the Patricia case in the context of the steady state assumption, as well as the time period selected would be useful.

**Reply: From Emanuel 2012: "Following E97, we assume that the time scale of tropical cyclone intensification is long enough that the vortex (above the boundary layer) can be considered to evolve through a sequence of quasi-balanced states for which the thermal wind equation, based on hydrostatic and gradient wind balance, always applies." We do assume that the vortex evolution is quasi-balanced, and the establishment of a critical Ri should be very fast compared to the vortex evolution time scale. Then the diagnosed V equation and the stratification of outflow temperature on M surfaces are also applicable in developing tropical cyclones. But, of course, the analytic solution of radial structure (equation (36) in ER11) using steady-state assumption (equation (16) in ER11) only applies to the steady state. The time we selected for Patricia evaluation is the observed peak intensity time (centered on an approximate 24h quasi-steady period). Although the intensification persists for another 12 hours in the WRF simulation, the storm is close to its quasi-steady state. We added some clarification in summary (L439-441).**

3. The Patricia simulation used 42 vertical levels with very course vertical resolution at the outflow. It would be useful to conduct an additional simulation with double vertical resolution to make sure that the analysis and conclusions are not dependent on the vertical resolution. Additionally, it would be useful to test the sensitivity of the model simulation results to the parameterization of turbulence at the outflow layer. Given the importance of the turbulence in the outflow layer for the theory, it would be useful to assess how critical the turbulence parameterization in the upper levels really is. Perhaps an additional simulation could be performed with a different turbulence parameterization in the outflow layer or perhaps making some meaningful (but realistic) changes to the existing parameterization in this region would be useful.

**Reply: The real case simulation is from a real-time data assimilation and forecasting system (PSU-EnKF system: http://www.adapt.psu.edu/index.php?loc=outreach) which needs to consider the consumption of computing resources and simulation speed. We agree with the reviewer that the vertical levels ~80 will be a better choice, which is the case for NOFLOW and SH5 (98 levels). The purpose to include a real case simulation is to check the agreement between the analytic theory and the real-case simulation in operational forecasts without further tuning (L99-101). We found that despite the rather moderate vertical resolution, the assumptions are approximately satisfied, and the simulated intensity is generally consistent with that predicted by the theory. To at least partially address the reviewer's concern about vertical resolution, we did also evaluate the sensitivity of vertical resolution in the assumptions of the ER11/ER12 theory for the two idealized simulations, which were originally conducted in Tao and Zhang (2014) that had only half the number of vertical layers. We did not find significant differences in the assessment of the assumptions and predicted intensity between the high vertical resolution simulations shown in the main text**

**and the coarser resolution simulations in Tao and Zhang (2014), which at least to some extent suggests the resilience of the ER11/ER12 theory (L135-138, L430-435).**

**The Vertical diffusivity coefficient of YSU PBL scheme depends on Ri in free stable atmosphere (Ri > 0):**

**$K_m = l^2 f(Ri)\sqrt{(\frac{\partial V_t}{\partial z})^2 + (\frac{\partial V_r}{\partial z})^2}$, in which $f(Ri) = \frac{1}{(1+5Ri)^2}$ (Figure R1).**

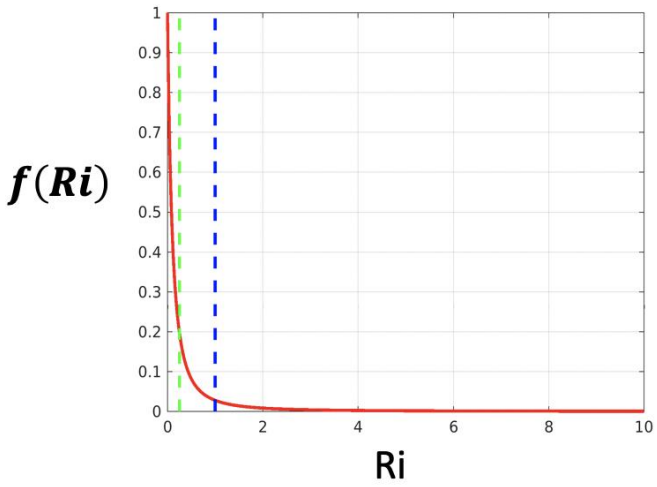


**Figure R1. $f(Ri)$. The blue dash line is Ri=1, while the green dash line is Ri=0.25.**

**The vertical diffusion exists with any value Ri > 0, which means there is no specific value for the critical Richardson number in YSU PBL scheme. As suggested by the reviewer, we did two sensitivity simulations of the turbulent parameterization by changing the YSU PBL scheme to introduce a critical Richardson number for the free atmosphere. Two sensitivity experiments for NOFLOW with Ric=0.25 and Ric=1 are performed (FigureR2). The change in YSU PBL scheme is to set $K_m = 10^{-8}$ $m^2$ $s^{-1}$ (no turbulence) when Ri >= Ric. The results for the selected times (Table R1 below) show that the storm reacts to the changes while holding the agreement between its structure and $\frac{\partial T_o}{\partial M}$ .**

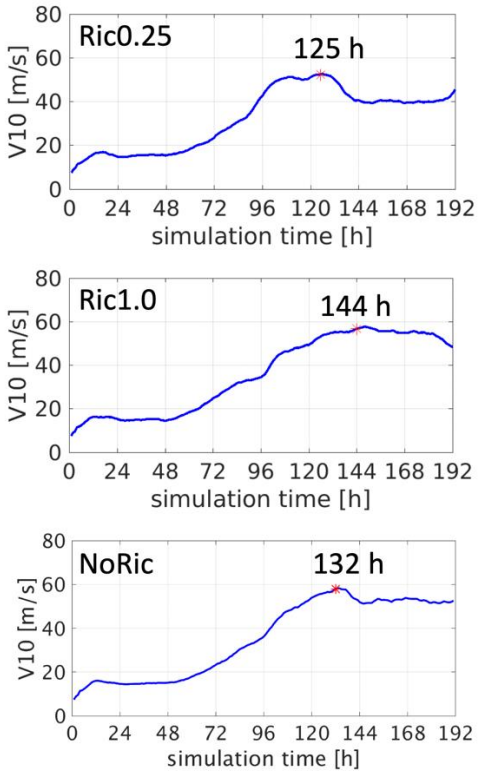


**Figure R2. Intensity evolution of the two simulations with a critical Richardson number of 0.25 (Ric0.25) and 1.0 (Ric1.0) and the simulation in the paper. The original YSU scheme is shown as NoRic.**

**Table R1. The outflow temperature stratification on M calculated using model simulations with and without $Ri_c$ for NOFLOW. Height of the boundary layer top: 1km. Column 2: radius of maximum wind at the top of the boundary layer. Column3: $M_{RMW}$. Column 4: $\frac{\partial M}{\partial r}$ at the radius of maximum wind and the top of the boundary layer. Column 5: the outflow temperature stratification on M predicted by equation (6) in the paper given the radial profile of tangential wind from the simulations, $T_b - T_{om} \sim 87$ K. Column 6: right hand side of equation (1) using $\frac{dM}{ds^*}$ from model output similar to Figure 4. Calculated the same way as Table 1 in the paper.**

| NOFLOW | $r_m$ [km] | $M_{RMW}$ [106 $m^2$ $s^{-1}$] | $\left.\frac{\partial M}{\partial r}\right\|_{r_m}$ [m $s^{-1}$] | $\left.\frac{\partial T_o}{\partial M}\right\|_{M_{RMW}}$ [$10^{-6}$ K s $m^{-2}$] | $-\frac{1}{r_m^2}(\frac{dM}{ds^*})$ [10-6 K s $m^{-2}$] |
|---|---|---|---|---|---|
| Ric0.25 at 125 h | 22 | 1.19 | 54.10 | 73.08 | 85.41 |
| Ric1.0 at 144 h | 22 | 1.33 | 62.40 | 61.33 | 64.17 |
| NoRic at 132 h | 20 | 1.21 | 56.47 | 85.00 | 93.67 |

**Specific Comments**

1. Section 2. Is there a sponge layer at the top of the model domains? If so, how deep is it and how is the sponge formulated. How far is the bottom of the sponge above the top of the outflow?
   **Reply: Yes, there are sponge layers at the top of the model domains. For Patricia, the sponge layer is the top 5 km (p_top = 10 hPa ~ 30 km height) with w-Rayleigh damping (damp_opt=3, for real-data cases); for NOFLOW and SH5, the sponge layer is between 20.5-24.5 km with Rayleigh damping (damp_opt=2, for idealized cases). All of the sponge layers are at least 5 km higher than the upper edge of the outflow region.**

2. Line 115. I think the simulation with no background flow could be referred to as SH0 instead of NOFLOW, since this is a companion to the SH5 simulation.
   **Reply: The name of 'NOFLOW' is following a series of papers with the same background-flow setup of simulations (Zhang and Tao 2013, Tao and Zhang 2014, 2015, 2019). There was a set of simulations with no shear but 2-m/s mean flow called SH0. For consistency, we would like to keep it as 'NOFLOW'.**

3. Lines 129-134. How is turbulence above the PBL computed?
   **Reply: The YSU PBL scheme represents all the vertical turbulence, while the km_opt represents the horizontal turbulence when diff_opt > 0 according to the WRF user guide. The advection scheme in WRF contains a higher-order filter which acts as horizontal diffusion to keep the simulation stable when explicit diffusions are off (diff_opt=0).**

4. Lines 174-175. Perhaps reword to "… the ER11 theory are both dependent on the …"
   **Reworded.**

5. Line 180. Could be reworded to "… super-gradient jet is missing…"
   **Reworded.**

6. Lines 203-204. Is the fact that the boundary layer top is a function of radius important here and how sensitive are the results to the selection of the boundary layer heights.
   **Reply: In this paper, the boundary layer top is selected at the height where the maximum gradient wind first agrees well with the maximum modeled tangential wind. The height of the selected boundary layer top will change the agreement between the diagnosed velocity/gradient wind and the modeled tangential wind inside the boundary layer. Since the height of the boundary layer top generally decreases with radius outside the RMW, the heights in the paper ensure that the radial wind profile of the modeled tangential wind will be all above the boundary layer where the gradient wind balance holds.**

7. Line 242. Is the definition of the Ri calculation identical to that used in the model parameterization? What is the critical Ri used in the model computation?

**Reply: In YSU PBL scheme, the calculation of Ri is the same as equation (3) for non-cloudy air, while in saturated regions the dry Brunt-Vaisala frequency is replaced by the moist one, but since the saturation mixing ratio is tiny in the outflow region, the two are virtually identical.**

**As shown in the answer to general comment 3, diffusion exists with any value Ri > 0, which means there is no specific value for the critical Richardson number in YSU PBL scheme. However, the diffusivity is a sensitive function of Ri and, empirically, the model tends toward a range of low but positive Ri (Figure R3 shows Ri tends to be in the range of [0 1]). So, while it does not conform explicitly to the conditions of ER11, it seems to qualitatively behave in a similar way. Since the critical Richardson number enters the equations in a form of $\frac{Ri_c}{{r_t}^2}$, which is then replaced by $\frac{{C_k}/{C_d}}{{r_m}^2}$, we can proceed with no specific value of the critical Richardson number.**

**We also did a small set of ensemble with random perturbation in the boundary layer mixing ratio (the same way we did in Tao and Zhang 2019) for NoRic. The Ric1.0 simulation falls within the ensemble spread which means there's no significant difference between Ric1.0 and NoRic (Figure R4) because $f(Ri)$ is very small when Ri > 1 (Figure R1).**

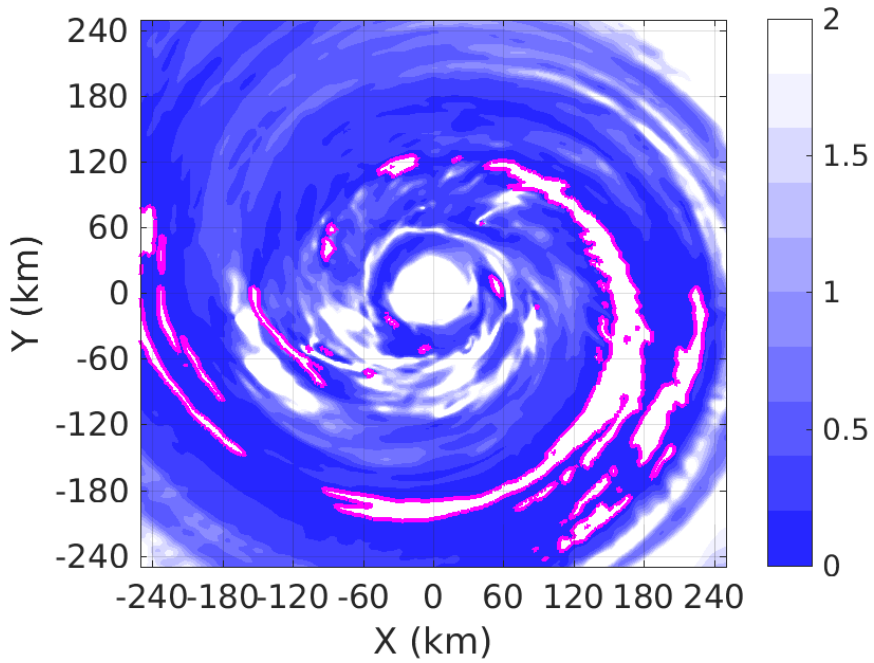


**Figure R3. Ri distribution at 13km of SH5 (132h). Magenta contours indicate Ri=0.**

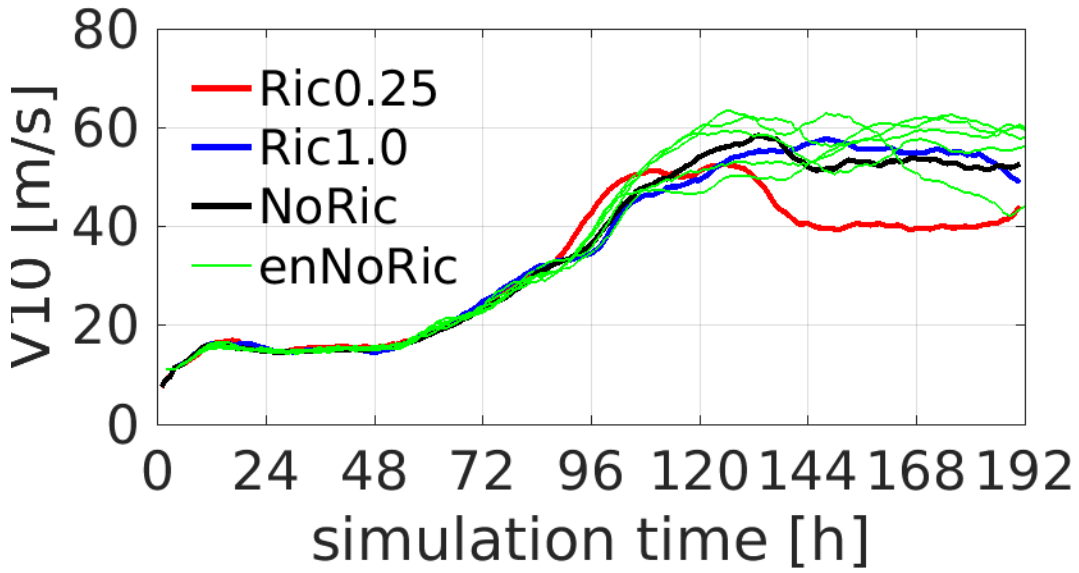


**Figure R4. Intensity evolution of Ric0.25 (red), Ric1.0 (blue), NoRic (black) and 5 members (green) from randomly perturbing the boundary layer mixing ratio of NoRic.**

8. P. 13, Lines 279-282. How does dominance of the radial wind in the outflow region impact the theory? I'm assuming it is mostly outside the MRMW, but what about right in the vicinity of MWRW?

**Reply: If we keep the radial wind component in Ri, follow equations (23) – (31) in ER11, we can finally get**

$$\left(\frac{\partial T_o}{\partial M}\right)_{with\ Vr} \cong \left[-1+\left(\frac{\partial V_r}{\partial z}\right)^2 {r_t}^2 \frac{ds^*}{d\mathrm{M}} \frac{\partial \mathrm{T}}{\partial s^*} \frac{1}{\Gamma_m} \left(\frac{\partial \mathrm{M}}{\partial \mathrm{z}}\right)^{-1}\right] \frac{Ri_c}{{r_t}^2} \left(\frac{dM}{ds^*}\right).$$

**Given $\frac{ds^*}{d\mathrm{M}} < 0$, $\frac{\partial \mathrm{T}}{\partial s^*} < 0$ and $\frac{\partial \mathrm{M}}{\partial \mathrm{z}} < 0$ in the outflow region, $\left(\frac{\partial T_o}{\partial M}\right)_{with\ Vr} \geq -\frac{Ri_c}{{r_t}^2}\left(\frac{dM}{ds^*}\right)$. Ignoring the radial component in vertical wind shear will lead to smaller $\frac{\partial T_o}{\partial M}$, hence, broader radial profile.**

9. P. 15, Lines 322-327. The normalized residuals are quite large at 25% and 50%. I don't consider a residual of less the 25% to be "small", in general. It would be helpful if the authors could justify more about the expected residual in the calculation that is used to support the self-stratification hypothesis.

**Reply: A simple estimation is shown below and in the paper (L360-364).**

**The expression of radial angular momentum profile without using $\frac{\partial T_o}{\partial M} \cong -\frac{Ri_c}{{r_t}^2}\left(\frac{dM}{ds^*}\right)$ is:**

$$\left(\frac{M}{M_{RMW}}\right)^{2-\frac{C_k}{C_d}} = \left(\frac{r_b}{r_m}\right)^2 \left(1-\frac{\Delta T}{(T_b - T_{om})}\right), \qquad (1)$$

**$M$ is the angular momentum at $r_b$, $T_b$ is the boundary layer top temperature, $T_{om}$ is the outflow temperature of the $M_m$ at V=0, $r_m$ is the radius of maximum wind at**

**the top of boundary layer, $\Delta T$ is the outflow temperature difference between $M$ and $M_m$.**

**If we apply the residual Re to (1), then**

$$\left(\frac{M_{Re}}{M_{RMW}}\right)^{2-\frac{C_k}{C_d}} = \left(\frac{r_b}{r_m}\right)^2 \left(1 - \frac{(1\pm \mathrm{Re})*\Delta T}{(T_b - T_{om})}\right). \quad (2)$$

**(2) divided by (1):** $\left(\frac{M_{Re}}{M}\right)^{2-\frac{C_k}{C_d}} = \left(1 - \frac{\pm \mathrm{Re}*\Delta T}{(T_b - T_{om} - \Delta T)}\right)$.

**For** $\frac{C_k}{C_d} = 1$, $T_b - T_{om} \sim 90K$, $\Delta T \sim 10K$ **(for M close to** $M_{RMW}$**),** $\frac{\pm \mathrm{Re}*\Delta T}{(T_b - T_{om} - \Delta T)} \sim \pm 0.125\mathrm{Re}$**, which is 3.125% change in V for Re=25%, 6.25% change in V for Re=50%. With increasing** $\Delta T$ **(M further away from** $M_{RMW}$**), this Re can increase the change in V.**

**The original Figure 10 is confusing at some point, so we replaced it with Table 1.**

10. Lines 324-348. How does air sea coupling impact the analysis of Ck/Cd here? The models are not coupled to an ocean model and does that make a difference for these calculations?

    **Reply: We regard the response of $\frac{C_k}{C_d}$ to air-sea coupling as a separate research topic. The Ck/Cd in the current model is parameterized to be a function of wind (Ck/Cd ~ 1 near $r_m$ for strong winds). The air-sea coupling will introduce more complicity into the sea surface temperature distribution and hence the surface fluxes.**

11. Figures. A number of figures use a yellow contour and this can be difficult to view. Can a different color be used in Figs. 2, 3, 6, 8, 9, 10? The yellow contour is visible at some points, but with a white background is not very visible.

    **Reply: The yellow contours are changed to darker orange contours.**

Reviewer #2: This paper assesses the validity of Emanuel and Rotunno's (2011) assumption of Richardson number criticality in the tropical cyclone outflow layer, and its effect on analytically derived maximum tangential wind speed. A real-data simulation of Hurricane Patricia (2015), and two other idealized simulations of tropical cyclones, exhibit sub-critical Richardson numbers in the upper-tropospheric outflow layer. The region of subcritical Richardson number was smaller in the simulation of Patricia than in the idealized simulations, which the authors attribute to lower vertical resolution in the real-data simulation than in the idealized runs. In all simulations, the gradient wind approximation is valid at inner radii outside of the boundary layer, and the evolution of the maximum tangential wind speed is well represented by the analytic model. Finally, the radial wind profiles derived from the analytic model are qualitatively similar to those from the simulations, although Hurricane Patricia's very compact inner core was not well represented. Overall, this is a well-executed and interesting assessment of the Emanuel and Rotunno theory using 3-dimensional, convection-allowing simulations, and I recommend acceptance with minor revisions.

**Minor comments:**

Line 111: WRF is already defined on Line 37.
**Reply: Deleted the duplication.**

Line 146: Why was a 40-h forecast from this model run used instead of a forecast (or analysis) from a later run of the real-time model?
**Reply: We want to keep the entire rapid intensification period of Patricia which will be used to check the time-dependent validity of the V equation (right column of Figure 5).**

Lines 177-180: The gradient wind approximation does not appear to capture Patricia's tangential wind structure in the midtroposphere outside of the ~80-km radius (compare the 20 m/s tangential wind contour in Figs. 2a,b). Is there a reason for this, and does this have any implications for the analytically derived radial wind profiles?
**Reply: We added an extra column showing the difference between the gradient wind and tangential wind. The difference is actually quite small (~3m/s, Figure 2c). The issue is mainly caused by the contour interval (10m/s) in the earlier version of the figure. In current version, the contour is changed to 5 m/s.**

Lines 279-283: The ratio does not appear to be large along Mrmw in the outflow region in Fig. 8d. Furthermore, the region of large ratio is very shallow. Is the contribution from radial shear really negligible in this region?
**Reply: The analytic theory uses $\frac{ds^*}{dM}$ at $r_t = \sqrt{r_m^2 \frac{C_d}{C_k} Ri_c}$ to estimate $\frac{\partial T}{\partial M}$ at V=0. The location of $r_t$ is around the transition region of the eyewall to outflow, where the vertical shear is dominated by tangential velocity. Inside the outflow region further away from the center, the vertical wind shear is mostly from radial velocity. If we keep the radial wind component in Ri, follow equation (23) – (31) in ER11, we can finally get**

$$\left(\frac{\partial T_o}{\partial M}\right)_{with\ Vr} \cong \left[-1 + \left(\frac{\partial v_r}{\partial z}\right)^2 {r_t}^2 \frac{ds^*}{dM} \frac{\partial T}{\partial s^*} \frac{1}{\Gamma_m} \left(\frac{\partial M}{\partial z}\right)^{-1}\right] \frac{Ri_c}{{r_t}^2} \left(\frac{dM}{ds^*}\right).$$

**Given $\frac{ds^*}{d\mathrm{M}} < 0$, $\frac{\partial \mathrm{T}}{\partial s^*} < 0$ and $\frac{\partial \mathrm{M}}{\partial \mathrm{z}} < 0$ in the outflow region, $(\frac{\partial T_o}{\partial M})_{with\ Vr} \geq -\frac{Ri_c}{{r_t}^2}(\frac{dM}{ds^*})$. Ignoring the radial component will actually lead to smaller $\frac{\partial T_o}{\partial M}$, and hence a broader radial profile. We added some clarification in paper (L311-313).**

Fig, 2: The green wind vectors are very difficult to read. Recommend changing their format so that inflow and outflow layers can be distinguished.

**Reply: We updated the figure color. The green wind vectors are replaced by black thick arrows.**

Reviewer #3: In this manuscript, three different numerical simulations (two ideal and one real) are compared to the theory of Emanuel and Rotunno (2011; ER11). The theory is compared to the numerical simulations in regard to: 1) the existence of slantwise neutrality, 2) maximum wind above the boundary layer, and 3) Richardson number criticality in the outflow region. Overall, this manuscript that helps assess the applicability of the ER11 theory to more realistic numerical simulations of hurricanes, and therefore would have value to the research community. This manuscript could be publishable subject to the minor revisions listed below.

**Minor Comments:**

In order to compare the numerical simulations to the ER11 theory, the numerical simulations should be run so as to minimize the errors (truncation, physical process representation, etc). Both the real and ideal simulations are somewhat deficient in this regard. In the real simulation, only 42 vertical levels are used leading to coarser vertical resolution (very important for this study, in which vertical gradients are calculated), and also a constant horizontal diffusivity is used instead of the Smagorinsky deformation-based mixing. The ideal simulations are deficient because they use coarser 2 km horizontal grid spacing. Ideally, the real simulation should be re-run with the vertical resolution of the ideal simulations, and the ideal simulations should be re-run with 1 km horizontal grid spacing. Since I realize this would be a major change, perhaps the authors could instead add some sentences discuss the possible impact of the model setups on the results, and perhaps add some sensitivity tests for the ideal simulations (perhaps run at 1km grid spacing) to show that the results for 2 km grid spacing are robust.

**Reply: We have a correction in the Patricia simulation that it actually has no explicit horizontal diffusion given diff_opt=0 (L110-112). We agree with the reviewer that the horizontal and vertical resolutions will influence the area coverage of small Ri numbers. Comparing the results from 1-km (domain 4) and 3-km (domain 3) Patricia simulations (Figure R5), we find that the results are quite comparable in different horizontal resolution simulations. The vertical resolution has more impact on the Richardson number (Figure R6): higher vertical resolution leads to smaller Richardson number in the outflow region at larger radius. Nevertheless, the transition region (radius < 100 km) has small Ri numbers. We added clarification in the text (L430-435).**

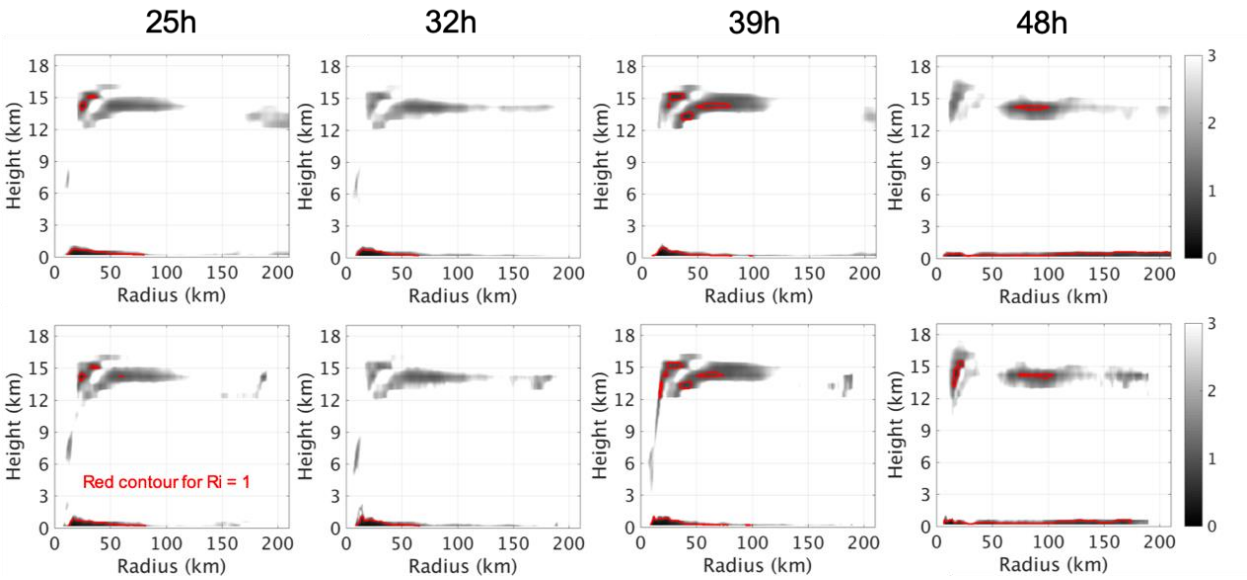


**Figure R5. Richardson number distribution in Patricia simulations with 3-km (upper row) and 1-km (lower row) horizontal grid spacings.**

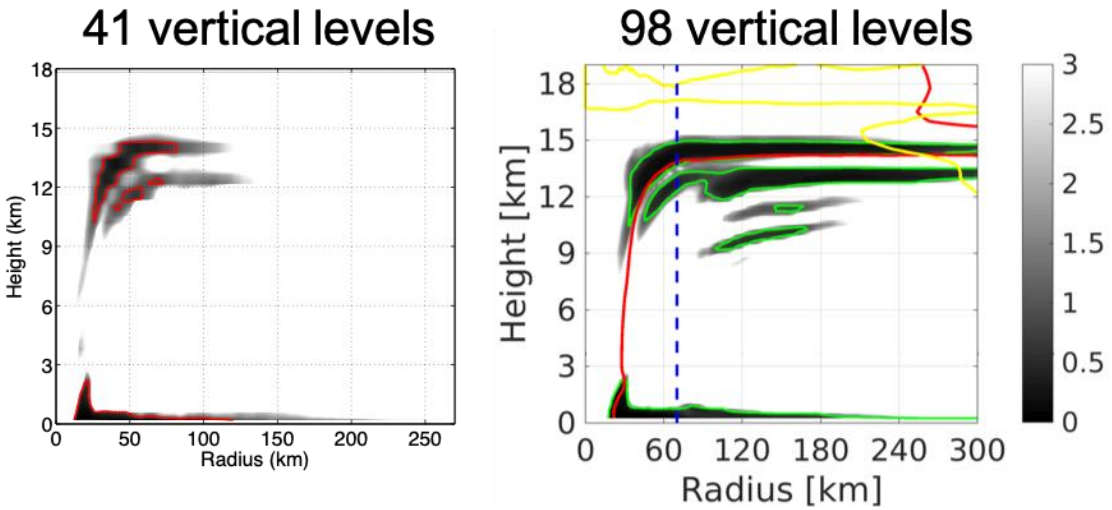


**Figure R6. Richardson number distribution in SH5 simulations with 41-vertical levels (left panel, Ric=1 in red) and 98-vertical levels (right panel, Ric=1 in green) at 132 h.**

The simulation with shear (SH5) appears to add little value to the paper. The simulation behaves very similar to the NOFLOW simulation, and there are some confusing results, such as a slightly stronger vortex. This does not make sense as vertical wind shear should weaken the vortex. It would be useful to re-run this simulation with a little stronger vertical wind shear (perhaps 7.5-10 m/s) to have a vortex with large asymmetries, and that is significantly weaker than the NOFLOW vortex. I am not convinced that shear is impacting this vortex in any significant way. **Reply: SH5 represents for a group of simulations with asymmetry (Figure R7) and showing that the theory can be applied to TCs with some asymmetry but with dominant axisymmetric mode. The reason for NOFLOW being weaker than SH5 is its secondary eyewall formation**

**(Figure 2d has some sign of the secondary eyewall), which hinders its further intensification (L155-156, L167-168).**

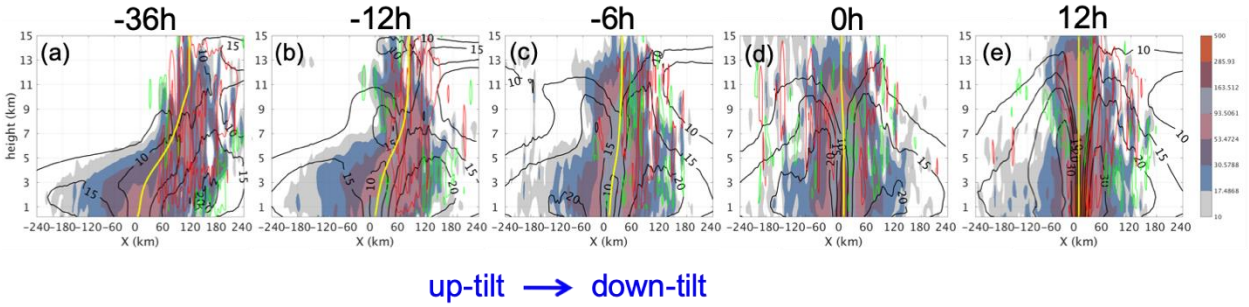


**Figure R7. Vertical cross-section plots of absolute vorticity (shading), vertical velocity (contours of [-1 -0.5 -0.3 -0.1 0.3 0.5 1 2 3 5] m/s, updraft in red, downdraft in green) and horizontal wind magnitude (black contours of [10 15 20 30 50 60] m/s) along tilt direction for SH5. The times are -36 h, -12 h, -6 h, 0 h and 12 h relative to the rapid intensification onset (RI onset = 0h). The yellow line is the approximate center line of the vortex column. Adapted from Figure 6 in Tao and Zhang 2019.**

**Tao, D. and F. Zhang, 2019: Evolution of Dynamic and Thermodynamic Structures before and during Rapid Intensification of Tropical Cyclones: Sensitivity to Vertical Wind Shear. Mon. Wea. Rev., 147, 1171–1191, https://doi.org/10.1175/MWR-D-18-0173.1**

L92: Please define the acronym "APSU"
**Reply: Rephrased the title to 'Deterministic forecast of Hurricane Patricia (2015) from Pennsylvania State University (PSU) real-time Hurricane Prediction System'.**

L102: I am surprised by the choice of only 42 vertical levels considering that you want to resolve sharp gradients in the upper troposphere. I think 60-80 levels would have been a better choice.
**Reply: The real case simulation is from a real-time data assimilation and forecasting system (PSU-EnKF system: http://www.adapt.psu.edu/index.php?loc=outreach) which needs to consider the consumption of computing resources and simulation speed. We agree with the reviewer that the vertical levels ~80 will be a better choice, which is the case for NOFLOW and SH5 (98 levels). The purpose to include a real case simulation is to check the agreement between the analytic theory and the real-case simulation in operational forecasts without further tuning (L99-101).**

L104: What is the motivation for using a horizontal diffusivity, instead of the more realistic Smagorinksy (km_opt=4)?
**Reply: We have a correction in the description of Patricia simulation that it actually has no explicit horizontal diffusion given diff_opt=0 (km_opt option will be ignored). It was used as default for the Penn State real-time WRF-EnKF hurricane analysis and prediction system. The advection scheme in WRF contains a higher-order filter which acts as horizontal diffusion to keep the simulation stable when explicit diffusions are off (diff_opt=0).**

L103-105: There is some confusion in this sentence. The YSU scheme solves a vertical diffusion equation with a vertical diffusivity. The constant that the authors refer to is the horizontal diffusivity I assume. Please clarify.
**Reply: We rephrased this part to 'The simulation uses the Yonsei University (YSU) boundary layer scheme (Hong et al. 2006) to represent the vertical turbulent mixing. The horizontal diffusion is implicitly included (diff_opt = 0 in WRF) in the advection scheme.'**

L115: Please specify what the vertical profile of vertical wind shear used was.
**Reply: We added clarification of the profile in the text (L122-125). Also, a reference is added for the vertical wind shear profile (Tao and Zhang 2014).**

**Tao, D., and F. Zhang, 2014: Effect of environmental shear, sea-surface temperature, and ambient moisture on the formation and predictability of tropical cyclones: An ensemble-mean perspective. J. Adv. Model. Earth Syst., 6, 384–404.**

L123: The domains DO NOT have horizontal resolutions of 18, 6, and 2 km. They have GRID SPACINGS of these values. With these grid spacings, features of 6*dx (~12 km on the finest mesh) and greater are decently resolved on the finest mesh. Please rephrase.
**Reply: Rephrased.**

L128: How many vertical levels were used for the idealized simulations?
**Reply: The idealized simulations have 98 vertical levels (L132).**

L149-151: Why does the simulation with shear have a stronger vortex than the simulation without shear? This goes against a ton of literature which states that on average hurricanes in shear should intensify slower and not be as intense. Yet, there is no discussion of this strange result. What is the purpose of running a simulation with shear, if the shear does not affect the vortex significantly?
**Reply: Generally speaking, TCs under shear would be weaker than TCs in a quiescent environment while holding other parameters the same (Figure R8). The weakening in the intensity of NOFLOW in this paper is due to a secondary eyewall formation (some sign of a secondary updraft at 40-km radius in Figure 2d), which hinders NOFLOW to reach an intensity higher than SH5. We clarified it in the text (L155-156, L167-168).**

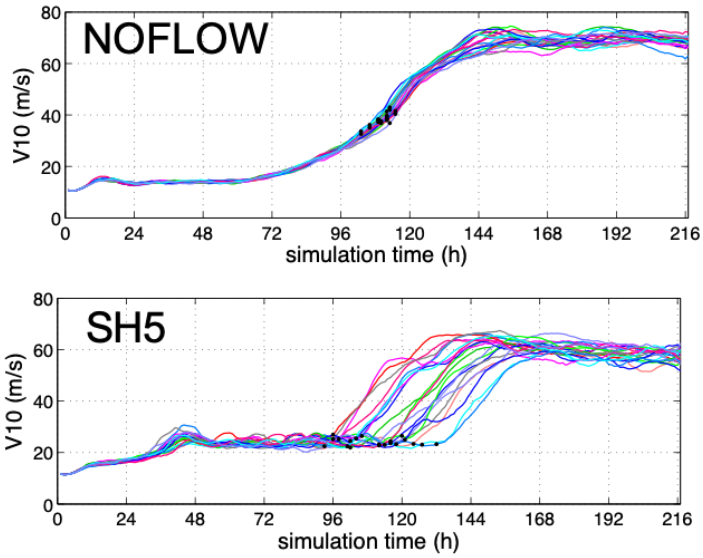


**Figure R8. Ensemble sets of NOFLOW and SH5. Adapted from Figure 1 in Tao and Zhang 2019.**

L154: The compactness of Patricia is due in part to the differences in horizontal grid spacings (1km vs. 2km). In this paper, I would suggest comparing each simulation individually to the ER11 theory, but not comparing the simulations to each other because the differences are due in part to the major differences in the model setups.

**Reply: We agree with the reviewer that the different resolutions influence the results, especially the distribution of small Ri in the outflow region. We pointed out this impact in several places (L135-138, L288-289, L430-435).**

L189: Undoubtedly, vertical resolution has something to do with this (this is again why it is important to have the model setups as similar as possible). This may not be physical. Also, please specify that you are referring to vertical locations (3 and 4.5 km).

**Reply: Specified in the text.**

L203: Please provide evidence that the top of the boundary layer are in fact 1.4, 1, and 1.5 km for the three simulations, respectively.

**Reply: We added an extra column in Figure 2 to show the difference between gradient wind and modeled tangential wind. The heights in the paper are selected as the location where the maximum gradient wind first agrees quantitatively with the maximum modeled tangential wind (L201-203).**

L224: What is the reason for the large variability for the theoretical Vt in SH5 and Patricia at the earlier times?

**Reply: At earlier times, the slantwise neutrality is not well established (L232-233). Especially in SH5, the shear has an effect on the TC structure to cause asymmetry before and even shortly after the rapid intensification onset (Figure R7 above).**

L261: In Figure 6, it is evident that both the vertical resolution and domain size differences are having an impact on the comparison. If the real domain was larger, I would assume the green area would extend farther out.

**Reply: We agree with the reviewer that the vertical resolution and domain size are having impacts on the coverage of the small Ri number. We have added some clarification in the text (L135-138, L430-435).**

Figure 2: If the innermost nest is 297x297, and the vortex is in the middle of the nest, there should only be values out to about 150 km. Why, then, in the real case, do the values extend to 180 km?

**Reply: We plot fields outside the radius of 135-km (Patricia) and 260-km (NOFLOW and SH5) using the data in the blue region (Figure R9) just for reference. We added dash white/black lines in figures to indicate this separation radius ($R_0$) and clarified in the figure caption.**

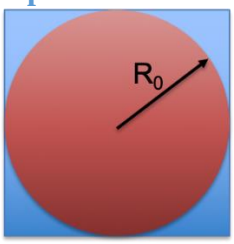


**Figure R9. Simple diagram showing the data coverage for the azimuthal average.**

Figure 2: It is very difficult to see the green vectors (magnitude and direction). Can fewer vectors be plotted, but slightly larger?

**Reply: We replotted the figure and replaced the green vectors with black solid arrows.**

Figure 2 (right): Wouldn't a difference field be better to show (vt-vg)? This might better illustrate the differences.

**Reply: The difference field is added in the third column.**

L232 and Figure 5: Shouldn't the ER11 theory be an upper bound on the azimuthal mean gradient wind from the simulations? Why do the simulations often exceed the theory? This is especially confusing for the SH5 case, in which a theory from the axisymmetric equations with no shear should have a larger predicted gradient wind than the simulation. Please provide a detailed explanation of this in the manuscript.

**Reply: The equation serving as upper bound on the azimuthal mean gradient wind is:**

$$V_{max}^2 = \frac{T_s - T_o}{T_s}\frac{C_k}{C_d}(k_s^* - k),$$

**in which $k_s^*$ is the specific enthalpies of air at saturation at sea surface temperature, and $k$ is the specific enthalpies of boundary layer air. In this equation, the third term of enthalpy flux through the top of the boundary layer ( $F_b$ ) in entropy tendency equation ( $h\frac{ds}{dt} =$**

**$\frac{1}{T_s}[C_k|V|(k_s^* - k) + C_d|V|^3 + F_b]$) is ignored, which usually has negative effect on entropy. Note that this quantity is NOT graphed in Figure 5. The diagnose equation (3) in paper is using the actual $\frac{ds^*}{dM}$ value from the model output data which includes the effect of $F_b$. Thus, it is not an upper bound.**

L232: It would useful to provide some support for the phrase "large asymmetry" in SH5 by showing a few plan-view plots. I am not convinced that SH5 has large asymmetries, and that shear is disrupting this simulation in any significant way, since the evolution is so similar to NOFLOW. Generally, some analysis of the level of asymmetries in each simulation would be beneficial since I assume ER11 should compare best to the simulations that have the least amount of asymmetries (see last general comment as well).
**Reply: Yes, ER11 is developed for axisymmetric storms. We added a reference in L157-159 which shows the difference between NOFLOW and SH5.**

**Tao, D. and F. Zhang, 2019: Evolution of Dynamic and Thermodynamic Structures before and during Rapid Intensification of Tropical Cyclones: Sensitivity to Vertical Wind Shear. Mon. Wea. Rev., 147, 1171–1191, https://doi.org/10.1175/MWR-D-18-0173.1**

General comment: Please provide some more motivation on how the ER11 theory (derived from the axisymmetric equations) can be used in comparisons to azimuthal mean quantities from 3D hurricane simulations (which have significant asymmetries). Perhaps, a brief review could be provided on all the assumptions of the ER11 theory (in addition to axisymmetry), and then a discussion on how the numerical simulations are similar or different from these assumptions.
**Reply: We added more discussion in L438-444.**

Revised paper with tracked changes

# Evaluation of the assumptions in the steady-state tropical cyclone self-stratified outflow using three-dimensional convection-allowing simulations

Dandan Tao[1, 2], Kerry Emanuel[3], Fuqing Zhang[1], Richard Rotunno[4], Michael M. Bell[2] and Robert G. Nystrom[1]

[1]Department of Meteorology and Atmospheric Science, and Center for Advanced Data Assimilation and Predictability Techniques, Pennsylvania State University, University Park, Pennsylvania

[2]Department of Atmospheric Science, Colorado State University, Fort Collins, Colorado,

[3]Program in Atmospheres, Oceans, and Climate, Massachusetts Institute of Technology, Cambridge, Massachusetts,

[4]National Center for Atmospheric Research, Boulder, Colorado

Corresponding author: Kerry Emanuel, emanuel@mit.edu

## ABSTRACT

The criteria and assumptions that were used to derive the steady-state tropical cyclone intensity and structure theory of Emanuel and Rotunno (2011) are assessed using three-dimensional convection-allowing simulations using the Weather Research and Forecasting model. One real-data case of Hurricane Patricia (2015) and two idealized simulations with and without vertical wind shear are examined. In all three simulations, the gradient wind balance is valid in the inner core region above the boundary layer. The angular momentum (M) and saturation entropy surfaces ($s^*$) near the top of the boundary layer, in the outflow region and along the angular momentum surface that passes the low-level radius of maximum wind ($M_{RMW}$) are nearly congruent, satisfying the criterion of slantwise moist neutrality in the vicinity of $M_{RMW}$. The theoretically derived maximum wind magnitude above the boundary layer compares well with the simulated maximum tangential wind and gradient wind using the azimuthally averaged pressure field during the intensification and quasi-steady state of the simulated storms. The Richardson number analysis of the simulated storms shows that small Richardson number ($0 < Ri \leq 1$) exists in the outflow region, related to both large local shear and small static stability. This criticality of the Richardson number indicates the existence of small-scale turbulence in the outflow region. We also show that the stratification of temperature along the M surface at the outflow region for steady-state hurricanes is approximately applicable in these 3-dimensional simulations, while the radial distribution of gradient wind is qualitatively comparable to the theoretical radial profiles. Some caveats regarding the theory are also discussed.

## 1. Introduction

The observed, nearly circular structure of mature tropical cyclones (TC) has motivated the development of the axisymmetric TC theory. Further assumptions of hydrostatic and gradient wind balance in the free atmosphere above the TC boundary layer, are supported by a scale analysis of the momentum and continuity equations (Willoughby 1979). In the series of papers, Emanuel (1986, 1997) developed a theory for steady-state TC's assuming hydrostatic and gradient wind balance above the boundary layer along with moist neutrality on constant absolute angular momentum (M) surfaces in the TC's inner core. In this potential intensity theory, the maximum gradient wind speed at the top of the boundary layer is related to the temperature difference between the boundary layer and outflow as well as the gradient of saturation entropy ($s^*$) across M surfaces. This theory also assumes that the streamlines emerging from the boundary layer all converge to a constant absolute temperature at the tropopause. However, Emanuel and Rotunno (2011, hereafter ER11) pointed out that the assumption of constant outflow temperature is not consistent with the results of numerically simulated tropical cyclones in which the temperature in the outflow region increases rapidly with M. In their revised theory (ER11; Emanuel 2012, hereafter E12), they proposed that the absolute temperature in the outflow region is not a constant, and that its stratification is determined by small-scale turbulence that limits the gradient Richardson number ($Ri$) to be near a critical value ($Ri_c$). Following these assumptions, they derived an equation for the outflow temperature as a function of M:

$$\frac{\partial T_o}{\partial M} \cong -\frac{Ri_c}{{r_t}^2}\left(\frac{dM}{ds^*}\right), \qquad (1)$$

where $T_o$ is the outflow temperature, $Ri_c$ is the critical Richardson number, $r_t$ is some physical radius in the outflow region. In ER11 and E12, this equation serves as an upper boundary condition

for the derivation of the balanced gradient wind radial profile in the TC's inner core above the boundary layer.

The Richardson number is the square of the ratio of the buoyancy frequency to the local vertical wind shear. Linear theory and laboratory experiments show an onset of turbulence when the gradient Richardson number falls below a critical value ($Ri_c$ = 0.25). Given that current resolution of models can only be used to calculate bulk Richardson number, this critical value is extended to 1 ($Ri_c$ = 1), which is often used as a threshold for the occurrence of parameterized small-scale turbulent mixing processes in models. The occurrence of $Ri$ criticality in real TCs has recently been studied by Molinari et al. (2014) and Duran and Molinari (2016), who found that the $Ri$ is indeed small in the outflow region of observed tropical cyclones. Both studies showed that low values of the Richardson number are frequent at around 13.5-km height within about 200-km radius, and that the altitude of the lowest $Ri$ steadily decrease with radius to a height of around 11.5 km at 1000 km away from the storm center. They attributed the frequent occurrence of low $Ri$ in the upper troposphere to both small static stability and large local vertical wind shear. They also found that weaker TCs have less frequent occurrences of low $Ri$ than hurricanes. These observational studies support the assumption of $Ri$ criticality in the outflow region of steady-state TCs proposed by ER11.

The basic insight of ER11 is that the TC outflow stratification embodied in $\frac{\partial T_o}{\partial M}$ is created by the TC itself and not determined by the environment. The purpose of this paper is to validate the assumptions used in ER11, to evaluate the diagnostic equation for the maximum gradient wind speed at the top of the boundary layer and also to compare the radial profile of the tangential/gradient wind at the boundary layer top to the one from ER11 self-stratification theory. Our evaluation of the ER11 assumptions uses three-dimensional simulations consisting of one real-

world case of Hurricane Patricia (2015), one idealized case of development in a homogeneous environment and another idealized case of development in a moderately sheared flow. Section 2 describes the experimental setup. Section 3 provides the overview of the three cases. Section 4 presents the results of checking the assumptions and comparing the predicted maximum gradient winds and radial profiles to those extracted from the model simulations. Summary and discussions are provided in Section 5.

## 2. Experimental Setup

### *2.1. Deterministic forecast of Hurricane Patricia (2015) from Pennsylvania State University (PSU) real-time Hurricane Prediction System*

Hurricane Patricia (2015) is a historic storm that broke several records (Rogers et al. 2017). The simulation of Hurricane Patricia (2015) analyzed in this study is the deterministic forecast generated by the PSU real-time Atlantic hurricane forecast and analysis system (Zhang et al. 2009, 2011; Zhang and Weng 2015; Weng and Zhang 2016). Here we are analyzing a model that was run in real time, not designing new simulations. The purpose of this real case is to test the agreement between the analytic theory and the real-case simulation in operational forecasts without further tuning. The simulation employed version 3.5.1 of Weather Research and Forecasting (WRF) model with an initial condition that included the assimilation of routine observations and airborne Doppler radar velocity, using the ensemble Kalman Filter method developed by Zhang and Weng (2015).

Four two-way nested domains are utilized with horizontal grid spacings of 27, 9, 3 and 1 km, which contain 378 × 243 for the outermost domain (D1), and 297 × 297 grid points for each of the inner three domains (D2-D4). There are 42 vertical model levels with the top level at 10 hPa

(~ 30 km) and a vertical grid spacing of about 0.9 km between z = 11-17 km. The simulation uses the Yonsei University (YSU) boundary layer scheme (Hong et al. 2006) to represent the vertical turbulent mixing. The horizontal diffusion is implicitly included (diff_opt = 0 in WRF) in the advection scheme. The surface fluxes of momentum and moist enthalpy are parameterized in terms of wind-dependent 'exchange coefficients' Cd and Ck, respectively, follows the recent study of Chen and Yu (2016) and Chen et al. (2018). A cumulus parameterization is used only for D1. The analysis in this paper is based on the simulation output from D4 with a 1-km horizontal grid spacing.

*2.2. Idealized simulations with high vertical resolutions*

The two idealized simulations were run using WRF version 3.9. Though the idealized simulations here use a newer version of WRF than that of the real-case simulation, there is no documented change in the fundamental model physics or performance between these two versions. One of the idealized experiments has no background flow (NOFLOW), while the other experiment has 5-m $s^{-1}$ westerly environmental shear (SH5) between 200 hPa and 850 hPa using a point down-scaling method that introduces vertical wind shear in the simulation without a horizontal temperature gradient (Nolan 2011). The vertical profiles of the background flows are shown in Figure 1 of Tao and Zhang (2014) that the shear is linear with height. The initial vortex is a modified Rankine vortex with a maximum surface wind speed of 15 m $s^{-1}$ at a 135-km radius. The domain is doubly periodic with a constant Coriolis parameter ($f = 5 \times 10^{-5}$ $s^{-1}$). The moist tropical sounding of Dunion (2011) is used to set up the thermodynamic environment, and both experiments have a constant sea-surface temperature of 27 °C. There are three two-way nested model domains, with domain sizes of 4320 km × 4320 km (D1), 1440 km × 1440 km (D2), and

720 km × 720 km (D3), and horizontal grid spacings of 18, 6 and 2 km, respectively. The model has 98 vertical levels with the model top at 24.5 km. The vertical grid spacing is around 0.3 km between z = 10-15 km. The vertical resolution in the outflow region in the idealized simulations is about 3 times higher than that in the real-case simulations, which will influence the magnitude of local vertical wind shear and hence the $Ri$ value (shown in Section 4.4). The $Ri$ value is sensitive to vertical grid spacings (dz = 0.3 km versus dz = 0.9 km in the outflow region) while horizontal resolution has little influence on the $Ri$ value (dx = 1 km versus dx = 3km) according to the comparisons between the results from simulations with different horizontal and vertical resolutions (not shown). Nevertheless, the fundamental physics behind the simulations should not have been altered.

As with the Patricia simulation, these simulations use YSU boundary layer scheme, WRF single-moment 6-class (WSM6) microphysics (Hong and Lim 2006). Different from the Patricia simulation, these idealized simulations use a simple horizontal diffusion option (diff_opt = 1 in WRF) with two-dimensional deformation (km_opt = 4 in WRF), no cumulus parameterization and no radiation schemes. The analysis of these idealized simulations in this paper is based on the simulation output from D3 with a 2-km horizontal grid spacing.

## 3. Overview of the three simulations

The maximum 10-m total wind evolutions are shown in **Figure 1**. The intensity from D4 of Hurricane Patricia (2015) simulation (PSU-d04) is reasonable compared to the best track data (**Figure 1a**). The rapid intensification and weakening are well captured by the model as well as the extreme intensity of 95 m $s^{-1}$. The rapid weakening in Patricia's intensity after 46 h is mainly due to its landfall.

NOFLOW and SH5 are idealized simulations starting from a weak cyclone. NOFLOW intensifies from 54 h to 136 h and weakens slightly due to a secondary eyewall formation afterward (not shown). The rapid intensification of SH5 starts at 90 h and ends at 122 h. The simulation reaches a quasi-steady state after the rapid intensification. The vortex structures of NOFLOW and SH5 at different stages are similar to their counterparts with a coarser vertical resolution (41 vertical levels) shown in Tao and Zhang (2019). NOFLOW has an axisymmetric structure at all times, while SH5 experiences episodes of strong asymmetry before the onset of rapid intensification (RI) but has persistently small asymmetry after RI onset.

We select the simulation results at 40 h (12 UTC of September 23, 2015) for Patricia and at 132 h for NOFLOW and SH5 as display times for Sections 4.1-4.2 and 4.4-4.6. The other times (Patricia: 20 h – 40 h; NOFLOW and SH5: 120 h – 180 h) give similar results for Sections 4.1-4.2 and 4.4-4.5 as the selected times and are not shown to avoid repetition. The maximum 10-m total wind speed of Patricia at 40 h is 92 m $s^{-1}$, while the maximum 10-m total wind speeds of NOFLOW and SH5 at 132 h are 58 m $s^{-1}$ and 62 m $s^{-1}$ respectively. NOFLOW has slightly weaker maximum intensity than SH5, which is associated with its secondary eyewall formation.

The left column of **Figure 2** shows the azimuthally averaged primary circulation and secondary circulation as well as the absolute angular momentum (M) for the three simulations at the selected times. Patricia (**Figure 2a**) has a compact primary circulation, with a surface radius of maximum azimuthally averaged tangential wind (RMW) of around 10 km. The 30-m $s^{-1}$ contour extends only to a radius of 55 km. The 10-m $s^{-1}$ contour reaches a height of 17 km, while the main outflow region is between z = 15 – 16.5 km. NOFLOW (**Figure 2d**) has a slightly larger primary circulation compared to Patricia. The surface RMW is around 18 km with the 30-m $s^{-1}$ wind contour extending to a radius of 90 km. The main outflow region is located between z = 13 – 15

177 km. SH5 (**Figure 2g**) has the largest primary circulation among the three cases with a surface
178 RMW of 22 km. The outflow height of SH5 is similar to NOFLOW.

179 The absolute angular momentum is defined as

180 $$M = rV_t + \frac{1}{2}fr^2, \qquad (2)$$

181 where $r$ is the radius to the surface center, $V_t$ is the azimuthally averaged tangential wind
182 calculated using the surface center, and $f$ is the Coriolis parameter. In Patricia, we simply use the
183 $f$ value at Patricia's surface center for calculation. Though $f$ changes with latitude, this difference
184 in calculating M and even the entire second term of (2) are negligible in the TC's inner core. The
185 M surface that passes surface RMW ($M_{RMW}$) follows the eyewall updrafts and then the outflow
186 region. In this paper, the region of interest is along $M_{RMW}$ and its vicinity. The $M_{RMW}$ contour will
187 act as a reference in the following sections.

188

189 **4. Results**

190 *4.1 Gradient Wind balance*

191 The maximum wind speed and radial profile derived from the ER11 theory are both
192 dependent on the gradient winds ($V_g$) at the boundary layer top. We first evaluate the assumption
193 of gradient wind balance. Using the azimuthally averaged pressure field from the model output,
194 the gradient wind is calculated and shown in the second column of **Figure 2**. The difference field
195 between $V_t$ and $V_g$ is shown in the third column of **Figure 2**. When compared to the azimuthally
196 averaged tangential wind from the model output, the gradient wind captures the structure and
197 magnitude within the TC inner core (radius < 100 km), above the boundary layer but below the
198 outflow region. In the boundary layer, the super-gradient jet is missing in the gradient wind
199 calculation as expected. The magnitude of the maximum gradient wind inside the boundary layer

is persistently smaller than the maximum tangential wind. In Sections 4.3 and 4.6, we use the altitudes where the maximum tangential winds first agree quantitively with the maximum gradient winds as the heights of the boundary layer top, which are z = 1.4 km for Patricia, z = 1 km for NOFLOW, and z = 1.5 km for SH5.

*4.2 Slantwise moist neutrality*

The ER11 theory assumes slantwise moist neutrality, which implies that the saturation entropy $s^*$ is a function of absolute angular momentum M alone ($s^* = s^*(M)$). This assumption is checked in **Figure 3**, in which the distributions of $s^*$ and M are shown. The calculation of saturation entropy uses the same equation as the equation (1) in ER11. From **Figures 3a-c**, we find that $s^*$ maximizes in the lower eye region (~ 3-km height in Patricia, ~ 4.5-km height in NOFLOW and SH5). The congruent M and $s^*$ surfaces are found in the lower boundary layer, the eyewall updrafts, and especially in the vast outflow region (**Figures 3b, d and f**). Hence, $s^*(M)$ is approximately satisfied in these quasi-steady-state TCs following the eyewall updrafts and the connected outflow. The assumption of the slantwise moist neutrality is thus reasonable in the vicinity of $M_{RMW}$. Outside the eyewall region, the M surfaces are nearly orthogonal to $s^*$ surfaces in the lower troposphere above the boundary layer.

*4.3 Evaluation of the diagnostic maximum gradient wind speed equation*

From hydrostatic and gradient balance as well as slantwise moist neutrality, the derived angular velocity equation at the top of the boundary layer is (the equation (13) of E12):

$$V^2 = -(T_b - T_o)M\frac{ds^*}{dM}, \qquad (3)$$

where $T_b$ is the temperature at the boundary layer top and $T_o$ is the outflow temperature where the tangential wind vanishes ($V_t$ = 0 m s$^{-1}$). To do the calculation from the azimuthally averaged fields of the three numerical simulations, we use $T_b$ on $M_{RMW}$ at the boundary layer top (z = 1.4 km for Patricia, z = 1 km for NOFLOW, and z = 1.5 km for SH5). For $T_o$, we use the outflow temperature on the $M_{RMW}$ at the location of $V_t$ = 0 m s$^{-1}$ (NOFLOW and SH5) or at the radius that reaches the farthest edge of the domain (135 km for Patricia). Because of the congruence of M and $s^*$ surfaces along $M_{RMW}$, $\frac{ds^*}{dM}$ should be constant on the $M_{RMW}$ surface above the boundary layer. In order to avoid the unwanted fluctuations and obtain a smoother V evolution from (3), $\frac{ds^*}{dM}$ is calculated using the linear regression coefficient of $s^*$ against M (**Figure 4**) in the outflow region. Generally speaking, the congruency of $s^*$ and M ensures their linear relationship, which can be used to get $\frac{ds^*}{dM}$. But in the early stages of development, $s^*$ and M surfaces are not well aligned even in the updraft region, as shown by Peng et al. (2018, 2019), which will lead to the poor results of $\frac{ds^*}{dM}$. To avoid imaginary values of V, we set $M\frac{ds^*}{dM}$ to zero wherever it is positive. The time-dependent values of $(T_b - T_o)$ and $M\frac{ds^*}{dM}$ as well as the diagnosed V are shown in **Figure 5**. Given the similar boundary layer top heights in Patricia and SH5, Patricia has a much larger temperature difference between the boundary layer top and the outflow region (95 K < $T_b - T_o$ < 105 K) than SH5 (80 K < $T_b - T_o$ < 85 K) during the quasi-steady state. The reason for this difference can be explained in two ways: one is that Patricia has a much higher outflow region than SH5 (**Figures 2a, g**); the other is that the tropopause temperature in Patricia is much lower than that in SH5 (will be shown in Section 4.5). The value of $(T_b - T_o)$ in NOFLOW is larger than SH5 mainly due to the lower boundary layer top. The time dependence of $(T_b - T_o)$ is mostly due to the increasing height of the outflow region during the intensification stage. However, the variance of $(T_b - T_o)$

contributes at most 15%[1] to the variance of V, which means the differences in V are mainly attributable to the differences in $M\frac{ds^*}{dM}$. **Figures 5b, e and h** show that, excluding the zeroed values near the beginning, $M\frac{ds^*}{dM}$ evolves from small values near 0 to ~ -75 $m^2\ s^{-2}\ K^{-1}$ in Patricia, to ~ -45 $m^2\ s^{-2}\ K^{-1}$ in NOFLOW and ~ -60 $m^2\ s^{-2}\ K^{-1}$ in SH5. Most of the intensification stages are captured in $M\frac{ds^*}{dM}$. The time dependence of $M\frac{ds^*}{dM}$ mostly comes from the entropy and absolute angular momentum distributions in the boundary layer which are highly related to the boundary layer dynamics as well as the surface exchange coefficients (it is not explicitly shown in (3), detailed derivation available in E12). From the right column of **Figure 5**, it is apparent that the diagnosed V is quantitatively comparable to $V_t$ and $V_g$ in all three simulations at all times after the storm is well developed, except for the early stage of SH5 when SH5 still has large asymmetry before the RI onset due to the vertical wind shear (Tao and Zhang 2019).

*4.4 Richardson number distribution*

The radial profile of the angular velocity at the boundary layer top in steady-state TCs developed in ER11 is about the role of small-scale turbulent mixing on setting the temperature stratification in the outflow region based on the critical Richardson number. When the Richardson number is smaller than this critical value, the flow is dynamically unstable and likely to initiate turbulent mixing. A classic way to parameterize the turbulence in numerical models uses $Ri_c$ = 1 as a threshold (no turbulence for $Ri \geq 1$, increasing eddy diffusivity for decreasing $Ri$ when $Ri < 1$). However, there is no specific critical value for $Ri_c$ in the free atmosphere for the WRF simulations with the YSU boundary layer scheme. The vertical diffusivity in the YSU boundary

[1] This number is simply calculated by $\max\left(\sqrt{\frac{(T_b - T_o)_{max}}{(T_b - T_o)_{min}}} - 1\right) \times 100\%$

layer scheme is a sensitive function of $Ri$ (equations A18 and A20 in Hong et al. 2006) and qualitatively behaves in a similar way as the classic turbulent parameterization for the free atmosphere. In this section, we will first check the distribution of the Richardson number and the existence of the Richardson number criticality ($0 < Ri \leq 1$) at the selected times. The Richardson number calculation used in this paper follows

$$Ri = \frac{N^2}{SH^2} = \frac{(\frac{g}{\theta_v})(\frac{\partial \theta_v}{\partial z})}{(\frac{\partial V_t}{\partial z})^2 + (\frac{\partial V_r}{\partial z})^2}, \quad (3)$$

where N is the Brunt–Väisälä frequency, a measure of the local static stability, $SH^2$ is the squared shear magnitude, $\theta_v$ is the virtual potential temperature, $V_t$ is the azimuthally averaged tangential wind, and $V_r$ is the azimuthally averaged radial wind. The calculation is based on the local vertical gradient of $\theta_v$ and shear, which indicates that the thicker the layer/model resolution, the more likely that large gradients will be averaged out in the small sub-regions of the layer of interest. Small positive Richardson number occur when the stratification is near neutral and/or when there is large vertical wind shear.

The $N^2$ distribution is shown in the first column of **Figure 6**. The $N^2$ values are small just below tropopause, and values greater than $3\times10^{-4}$ $s^{-2}$ only occur in a thin layer in the TC's eye below 3-km height, which corresponds to the large positive vertical gradient of $s^*$ in **Figures 3a, c and e**. Above the tropopause, the $N^2$ values are large, as expected. The distributions of shear magnitudes are shown in the second column of **Figure 6**. In all three cases, the shear magnitude maximizes in the boundary layer, the eyewall updrafts, and the outflow region, which is related to the structure of the TC tangential and radial flows (**Figure 2**). The corresponding low Richardson numbers ($0 < Ri \leq 1$) are found in the region where the eyewall updrafts intersect the outflow as well as in the boundary layer in all three cases. In NOFLOW and SH5, near-critical Richardson numbers are also found in the outflow regions extending out to radii larger than 260 km. In Patricia,

the coverage of small Richardson number in the outflow region is not as large as that in NOFLOW and SH5, which is due to a coarser vertical resolution at this height as described in Section 2. For a better sense of the magnitudes of $N^2$, squared shear and corresponding Richardson number, their vertical profiles at select radii are shown in **Figure 7**. From the vertical profiles, we conclude that the smaller Richardson numbers in these regions are the result of both large shear and small static stability which is consistent with the observational studies of Molinari et al. (2014) and Duran and Molinari (2016). The coarser vertical resolution of Patricia results in the smaller $SH^2$ in the outflow region (**Figure 7a**).

Given that the calculations of $N^2$, $SH^2$ and corresponding $Ri$ above are based on the azimuthally averaged fields and given that small-scale turbulent mixing happens locally in three dimensions, we further calculated the Richardson number at each grid point (x, y, z) and then checked the occurrence of the Richardson number criticality ($0 < Ri \leq 1$) along the azimuth at a given radius and height $(r, z)$. In the left column of **Figure 8**, the high frequency (percentage > 60%) of the Richardson number criticality in azimuth matches well with the critical Richardson number distribution simply using the azimuthally averaged fields (**Figures 6c, f and i**). This indicates that the approximation of axisymmetry for representing the three-dimensional fields works well for TCs in a quasi-steady state.

In deriving the relationship between M and $Ri$ in ER11, the radial flow contribution to the shear is neglected. In order to evaluate this approximation, we calculated the ratio of $(\frac{\partial V_t}{\partial z})^2$ to $(\frac{\partial V_t}{\partial z})^2 + (\frac{\partial V_r}{\partial z})^2$. A large ratio validates the assumption. The result (right column of **Figure 8**) shows that the contribution of the tangential wind is dominant in the area inside the eyewall and along $M_{RMW}$ in the outflow region, while the contribution of the radial wind is dominant in the boundary layer and in the outflow region away from $M_{RMW}$. Thus, this approximation validates in

311 the vicinity of $M_{RMW}$. Neglecting the contribution of radial wind in the shear actually leads to
312 smaller values of $\frac{\partial T_o}{\partial M}$, which can result in a broader radial profile of the angular velocity above the
313 boundary layer.

314 In this section, we have confirmed the $Ri$ criticality in the outflow region near $M_{RMW}$,
315 which indicates the existence of small-scale turbulent mixing in this area in 3-D model simulations.
316 Though there is no specific value for $Ri_c$ in the YSU boundary layer scheme, the model evolves
317 toward a range of low but positive $Ri$ $(0 < Ri \leq 1)$ in the outflow region, in qualitative
318 accordance with the assumption of $Ri$ criticality in the outflow region.

319

320 *4.5 Outflow temperature stratification in M coordinates*

321 The azimuthally averaged absolute temperature field and M surfaces are shown in the left
322 column of **Figure 9**. The eye temperature inside $M_{RMW}$ is clearly higher than the temperature
323 outside $M_{RMW}$ showing the existence of warm core. The horizontal gradient of the temperature
324 across the eyewall is considerably sharper in Patricia than those in NOFLOW and SH5 which is
325 consistent with the smaller scale of Patricia's inner core and its higher intensity. Another
326 interesting feature worth mentioning is the much colder tropopause temperature in Patricia, which
327 partly contributes to its higher intensity as discussed in Section 4.3. The stratification of outflow
328 temperature is quite obvious in **Figures 9a, d and g** that the M surfaces in the outflow region span
329 over a range of absolute temperature values. A clearer way to display this stratification is shown
330 in the middle and right columns of **Figure 9**, in which the M surfaces calculated from azimuthally
331 averaged tangential wind are plot as a function of azimuthally averaged tangential wind and
332 azimuthally averaged absolute temperature. The region that this temperature stratification builds
333 up is highlighted in the magenta box in the left panels of **Figure 9** and yellow contours of the

corresponding M surfaces in the right panels of **Figure 9**. The magnitude of $\frac{\partial T_o}{\partial M}$ is largest in Patricia while Patricia has the most compact structure among the three.

Given the assumptions of gradient wind balance, hydrostatic balance and slantwise moist neutrality, the self-stratification theory proposes that the outflow temperature stratification across M surfaces can be expressed by (1) in the introduction (the same as equation (31) in ER11). As stated in Section 4.4, subcritical Richardson numbers indicate the onset/existence of small-scale turbulence. Once the flow becomes turbulent, the Richardson number should be held near a critical value. By assuming the Richardson number in the outflow is near a critical value at some physical radius $r_t$, the temperature stratification calculated by (1) at $r_t$ is then approximately used to represent the $\frac{\partial T_o}{\partial M}$ at $V_t$ = 0 m s$^{-1}$, which acts as an upper boundary condition to derive the radial profile of gradient wind above the boundary layer. In ER11, $\frac{Ri_c}{{r_t}^2}$ is replaced by

$$\frac{Ri_c}{r_t^2} = \frac{C_k}{C_d}\frac{1}{r_m^2}, \qquad (4)$$

where $r_m$ is the radius of maximum wind at the boundary layer top.

Following the ER11 derivation but without using (1), the outflow temperature as a function of M is expressed as

$$\frac{T_o(M)-T_{om}}{(T_b-T_{om})} = 1 - \left(\frac{M}{M_{RMW}}\right)^{2-\frac{C_k}{C_d}} / \left(\frac{r}{r_m}\right)^2. \qquad (5)$$

of which $T_{om}$ is the outflow temperature on $M_{RMW}$, $T_b$ is the boundary layer top temperature (assumed to be a constant with radius) and $T_o(M)$ is the outflow temperature on M. By taking $\frac{\partial}{\partial M}$ of (5), we get the stratification of the outflow temperature with respect to M without using (1):

$$\left.\frac{\partial T_o}{\partial M}\right|_{M_{RMW}} = \frac{(T_b-T_{om})}{M_{RMW}}\left(\frac{2}{r_m}\frac{M_{RMW}}{\left.\frac{\partial M}{\partial r}\right|_{r_m}} - 1\right), \qquad (6)$$

where we use $\frac{C_k}{C_d} = 1$, $r = r_m$ and $M = M_{RMW}$.

We evaluate (1) as follows: firstly, we use (6) to calculate the outflow temperature stratification with respect to M given the radial profile of modeled tangential wind above the boundary layer (the fifth column of Table 1); secondly, we calculate the right-hand side of (1) using (4) and $\frac{C_k}{C_d} = 1$ at the boundary layer top (the last column of Table 1). The values of each term from the three simulations are listed in Table 1.

The values of $\frac{\partial T_o}{\partial M}$ calculated from two methods with and without (1) agree well with each other, yielding a difference less than 20%, which is equivalent to a difference in M(r) of around 3% for M surfaces near $M_{RMW}$ (evaluated from (5)). Therefore, equation (1) is approximately satisfied in the expected region, thus the self-stratification hypothesis is qualitatively consistent with the simulations of the three quasi-steady-state TC cases.

*4.6 Radial structure of the wind at the boundary layer top*

The stratification of the outflow temperature is finally used to derive the analytical solution of the steady-state radial structure of the gradient wind at the boundary layer top in ER11. The V(r) is in form of angular momentum:

$$\left(\frac{M}{M_{RMW}}\right)^{2-(C_k/C_d)} = \frac{2(r/r_m)^2}{2-(C_k/C_d)+(C_k/C_d)(r/r_m)^2}. \quad (7)$$

In order to get this analytical solution, some further assumptions are made:

1. $C_k/C_d$, $T_b$, $\frac{Ri_c}{{r_t}^2}$, sea surface saturation entropy ($s_0^*$) are constants;
2. entropy and angular momentum are well mixed in the boundary layer that $\frac{ds^*}{dM}$ at the surface can be used to represent the $\frac{ds^*}{dM}$ at the boundary layer top.

375 Using (1) together with the gradient wind balance and slantwise moist neutrality while
376 neglecting the Coriolis terms in the inner core and maximizing V at $r_m$, we can derive the radial
377 distribution of the gradient wind speed for steady-state tropical cyclones above the boundary layer
378 as presented in (7).

379 **Figure 10** compares the radial profiles of model derived azimuthally averaged tangential
380 wind speed, gradient wind speed calculated from azimuthally averaged pressure field and
381 analytical solution from the simplified model. The analytical solution with $\frac{C_k}{C_d} = 0.5$ has the
382 broadest profile with respect to $r/r_m$. With larger $\frac{C_k}{C_d}$, the analytical solution becomes more
383 compact. The radial wind profiles of Patricia and SH5 derived from the model simulations tend to
384 be more compact than the analytical solutions with $\frac{C_k}{C_d}$ in a reasonable range of [0.5, 1.5] (Bell et
385 al. 2012) inside ~ 6RMW. The radial profile of the tangential wind in NOFLOW outside RMW
386 decays more slowly than that in Patricia and SH5, which is closer to the analytical solution. This,
387 however, is due to the broadening of the wind field before the secondary eyewall formation
388 (secondary updrafts near 40-km radius shown in **Figure 2d**) in NOFLOW.

389 The discrepancies in the profiles are not surprising in view of the assumptions to derive the
390 analytical solution. First of all, $\frac{C_k}{C_d}$ in the model is not constant with radius (decreasing with radius
391 outside the eyewall region in these simulations). Secondly, the assumption that the boundary layer
392 is well mixed, which is however not the case as shown in many studies (Zhang et al. 2011, Kepert
393 et al. 2016), will introduce some deviation of the analytical solution from the modeled $\frac{ds^*}{dM}$ and
394 hence the radial profile. Thirdly, the 3-dimensional simulations have an additional dimension of
395 freedom compared to axisymmetric models, permitting asymmetries at all scales that can have an
396 impact on the distribution of surface fluxes and stress (hence $s^*$ and M in the boundary layer) as

well as the storm structure. Besides the discrepancies in the parameters, neglecting the radial component of the vertical shear in the derivation of ER11 and the gradient of temperature with respect to $s^*$ in pressure coordinates (first term on the right-hand side of equation (29) in ER11) will lead to smaller $\frac{\partial T_o}{\partial M}$. Given the smaller $\frac{\partial T_o}{\partial M}$ used in the analytic solution, the radial profile of angular velocity can be expected to be broader than the modeled radial profile. Nevertheless, the analytical solution and its derivation process are beneficial for understanding tropical cyclones from both the dynamic and thermodynamic aspects as well as giving insights on the connection of the outflow region and the boundary layer dynamics. Generally speaking, the analytical solution gives a plausible approximate radial profile for the tangential wind above the boundary layer for mature tropical cyclones.

## 5. Summary and conclusions

Three simulations (one deterministic forecast of Hurricane Patricia, one idealized case with no background flow and one idealized case with vertical wind shear) are used to evaluate the assumptions used in ER11, the diagnosed maximum gradient wind at the boundary layer top and the analytical solution of the radial profile for gradient wind above the boundary layer. The three cases are representative of three groups of TCs: real TCs with asymmetries and strong environmental influences, TCs in idealized homogeneous environment with near-axisymmetric structures, and TCs in idealized sheared environments with asymmetries.

The diagnosed maximum gradient wind at the boundary layer top using (3) is quantitatively comparable to the modeled maximum azimuthally averaged tangential wind and gradient wind calculated from the azimuthally averaged pressure field after an initial organization stage, when the congruence of $s^*$ and M surfaces becomes established, as shown by Peng et al. (2018). One

important thing to emphasize is that the diagnosed maximum V from (3) is for the gradient wind, while the model simulated flow can be super-gradient within the boundary layer. For the three cases in this study, the diagnosed maximum V is consistently smaller than the modeled maximum tangential wind $V_t$ but comparable to the maximum gradient wind $V_g$ within the boundary layer, as expected (**Figures 2c, f and i**).

In the three cases studied in this paper, the slantwise moist neutrality assumption is satisfied along the $M_{RMW}$ surface from the boundary layer top through the outflow region. Near-critical Richardson numbers are found in the outflow region along $M_{RMW}$, resulting from the large vertical wind shear and the reasonably small Brunt–Väisälä frequency in the upper troposphere. The criticality of Richardson numbers in the outflow region indicates the existence of small-scale turbulent mixing. We also analyzed several simulations with the same setups but different vertical and horizontal grid spacings (not shown), and found that the degree of Richardson number criticality in the outflow region is closely related to the model resolutions, especially the vertical resolution. The higher model resolution (mainly vertical), the larger the area of Richardson number criticality. However, the region where the updrafts transition to the outflow always has small Richardson number.

The results of this analysis support the hypothesis of ER11 and E12 that the intensity and structure of tropical cyclones partially depend on the stratification of the outflow temperature. Equation (1) gives a plausible estimate of the outflow temperature stratification on M surfaces at $V_t$ = 0 m s$^{-1}$, which is used to further derive (7). The analyses in Sections 4.2-4.5 also works for developing storms with established slantwise neutrality, while the analytical solution given by (7) is for steady-state tropical cyclones (steady-state assumption is used during derivation). The simulated radial structure of tangential wind at the boundary layer top is broadly consistent with

the analytic solution based on the assumption of criticality in the outflow region, but there are some discrepancies due to simplifications in the analytic model as described in Section 4.6. Further analysis of how the outflow temperature stratification evolves and analysis of the theoretical assumptions in the boundary layer will be studied in follow-up research.

**Acknowledgements**:*:* Authors Tao and Zhang were partially supported by NSF Grant AGS-1305798, ONR Grant N000140910526, and NOAA HFIP. Robert Nystrom was supported by NASA Grant 17-EARTH17F-184. Kerry Emanuel was supported by the Office of Naval Research under grant ONR N00014-18-1-2458. The contribution of R. Rotunno to this work is supported by the National Center for Atmospheric Research, which is a major facility sponsored by the National Science Foundation under Cooperative Agreement No. 1852977. Computing was performed at the Texas Advanced Computer Center.

**References:**


Bell, M.M., M.T. Montgomery, and K.A. Emanuel, 2012: Air–Sea Enthalpy and Momentum Exchange at Major Hurricane Wind Speeds Observed during CBLAST. *J. Atmos. Sci.*, **69**, 3197–3222, https://doi.org/10.1175/JAS-D-11-0276.1

Chen, Y., and X. Yu, 2016: Enhancement of wind stress evaluation method under storm conditions. *Climate Dyn*., **47**, 3833–3843, https://doi.org/10.1007/s00382-016-3044-4.

Chen, Y., F. Zhang, B. W. Green, and Y. Xu, 2018: Impacts of Ocean Cooling and Reduced Wind Drag on Hurricane Katrina (2005) Based on Numerical Simulations. *Monthly Weather Review*, **146**, 287-306, https://doi.org/10.1175/MWR-D-17-0170.1

Dunion, J. D., 2011: Rewriting the climatology of the tropical North Atlantic and Caribbean Sea. *J. Climate*, **24**, 893–908, https://doi.org/10.1175/2010JCLI3496.1.

Dudhia, J., and Coauthors, 2008: Prediction of Atlantic tropical cyclones with the Advanced Hurricane WRF (AHW) model. Preprints, 28th Conf. on Hurricanes and Tropical Meteorology, Orlando, FL, Amer. Meteor. Soc., 18A.2. [Available online at https://ams.confex.com/ams/28Hurricanes/techprogram/ paper_138004.htm.]

Duran, P. and J. Molinari, 2016: Upper-Tropospheric Low Richardson Number in Tropical Cyclones: Sensitivity to Cyclone Intensity and the Diurnal Cycle. *J. Atmos. Sci*., **73**,545–554, https://doi.org/10.1175/JAS-D-15-0118.1

Emanuel, K. A., 1986: An air–sea interaction theory for tropical cyclones. Part I: Steady-state maintenance. *J. Atmos. Sci*., **43**, 585–604, https://doi.org/10.1175/1520-0469(1986)043,0585: AASITF.2.0.CO;2.

——, 1997: Some aspects of hurricane inner-core dynamics and energetics. *J. Atmos. Sci*., **54**, 1014–1026, https://doi.org/ 10.1175/1520-0469(1997)054,1014:SAOHIC.2.0.CO;2.

480 ——, 2012: Self-stratification of tropical cyclone outflow. Part II: Implications for storm
481 intensification. *J. Atmos. Sci*., **69**, 988–996, https://doi.org/10.1175/JAS-D-11-0177.1.
482 ——, and R. Rotunno, 2011: Self-stratification of tropical cyclone outflow. Part I: Implications
483 for storm structure. *J. Atmos. Sci*., **68**, 2236–2249, https://doi.org/10.1175/JAS-D-10-
484 05024.1
485 Hong, S.-Y., and J.-O. J. Lim, 2006: The WRF single-moment 6-class microphysics scheme
486 (WSM6). *J. Korean Meteor. Soc*., **42**, 129–151.
487 ——, Y. Noh, and J. Dudhia, 2006: A new vertical diffusion package with an explicit treatment of
488 entrainment processes. *Mon. Wea. Rev*., **134**, 2318–2341.
489 Kepert, J. D., J. Schwendike, and H. Ramsay, 2016: Why is the Tropical Cyclone Boundary Layer
490 Not "Well Mixed"?. *J. Atmos. Sci*., **73**, 957–973, https://doi.org/10.1175/JAS-D-15-
491 0216.1
492 Molinari, J., P. Duran, and D. Vollaro, 2014: Low Richardson Number in the Tropical Cyclone
493 Outflow Layer. *J. Atmos. Sci*., **71**, 3164–3179, https://doi.org/10.1175/JAS-D-14-0005.1
494 Nolan, D. S., 2011: Evaluating environmental favorableness for tropical cyclone development with
495 the method of point down-scaling. *J. Adv. Model. Earth Syst*., **3**, M08001, doi:10.1029/
496 2011MS000063.
497 Peng, K., R. Rotunno, and G. H. Bryan, 2018: Evaluation of a Time-Dependent Model for the
498 Intensification of Tropical Cyclones. *J. Atmos. Sci*., **75**, 2125–2138,
499 https://doi.org/10.1175/JAS-D-17-0382.1
500 ——, ——, ——, and J. Fang, 2019: Evolution of an Axisymmetric Tropical Cyclone before
501 Reaching Slantwise Moist Neutrality. *J. Atmos. Sci*., https://doi.org/10.1175/JAS-D-18-
502 0264.1

Rogers, R. F., S. Aberson, M. M. Bell, D. J. Cecil, J. D. Doyle, T. B. Kimberlain, J. Morgerman, L. K. Shay, and C. Velden, 2017: Rewriting the Tropical Record Books: The Extraordinary Intensification of Hurricane Patricia (2015). *Bull. Amer. Meteor. Soc*., **98**, 2091–2112, https://doi.org/10.1175/BAMS-D-16-0039.1

Tao, D., and F. Zhang, 2014: Effect of environmental shear, sea-surface temperature, and ambient moisture on the formation and predictability of tropical cyclones: An ensemble-mean perspective. *J. Adv. Model. Earth Syst*., **6**, 384–404, doi: 10.1002/2014MS000314.

——, ——, 2019: Evolution of Dynamic and Thermodynamic Structures before and during Rapid Intensification of Tropical Cyclones: Sensitivity to Vertical Wind Shear. *Mon. Wea. Rev.*, **147**, 1171–1191, https://doi.org/10.1175/MWR-D-18-0173.1

Willoughby, T. M., 1979: Forced secondary circulations in hurricanes. *J. Geophys. Res*., **84**, 3173-3183, doi:10.1029/JC084iC06p03173.

Zhang, F., and Y. Weng, 2015: Predicting hurricane intensity and associated hazards: A five-year real-time forecast experiment with assimilation of airborne Doppler radar observations. Bull. Amer. Meteor. Soc., 96, 25–32, doi:10.1175/ BAMS-D-13-00231.1.

——, ——, J. A. Sippel, Z. Meng, and C. H. Bishop, 2009: Cloud- resolving hurricane initialization and prediction through assimilation of Doppler radar observations with an ensemble Kalman filter: Humberto (2007). *Mon. Wea. Rev*., **137**, 2105–2125, doi:10.1175/2009MWR2645.1.

——, ——, J. F. Gamache, and F. D. Marks, 2011: Performance of convection-permitting hurricane initialization and prediction during 2008–2010 with ensemble data assimilation of inner- core airborne Doppler radar observations. *Geophys. Res. Lett*., **38**, L15810, doi:10.1029/2011GL048469.

526 Zhang, J. A., R. F. Rogers, D. S. Nolan, J. Marks, and D. Frank, 2011: On the characteristic height
527 scales of the hurricane boundary layer. *Mon. Wea. Rev.*, **139**, 2523–2535, doi:10.1175/
528 MWR-D-10-05017.1.

Figure 1



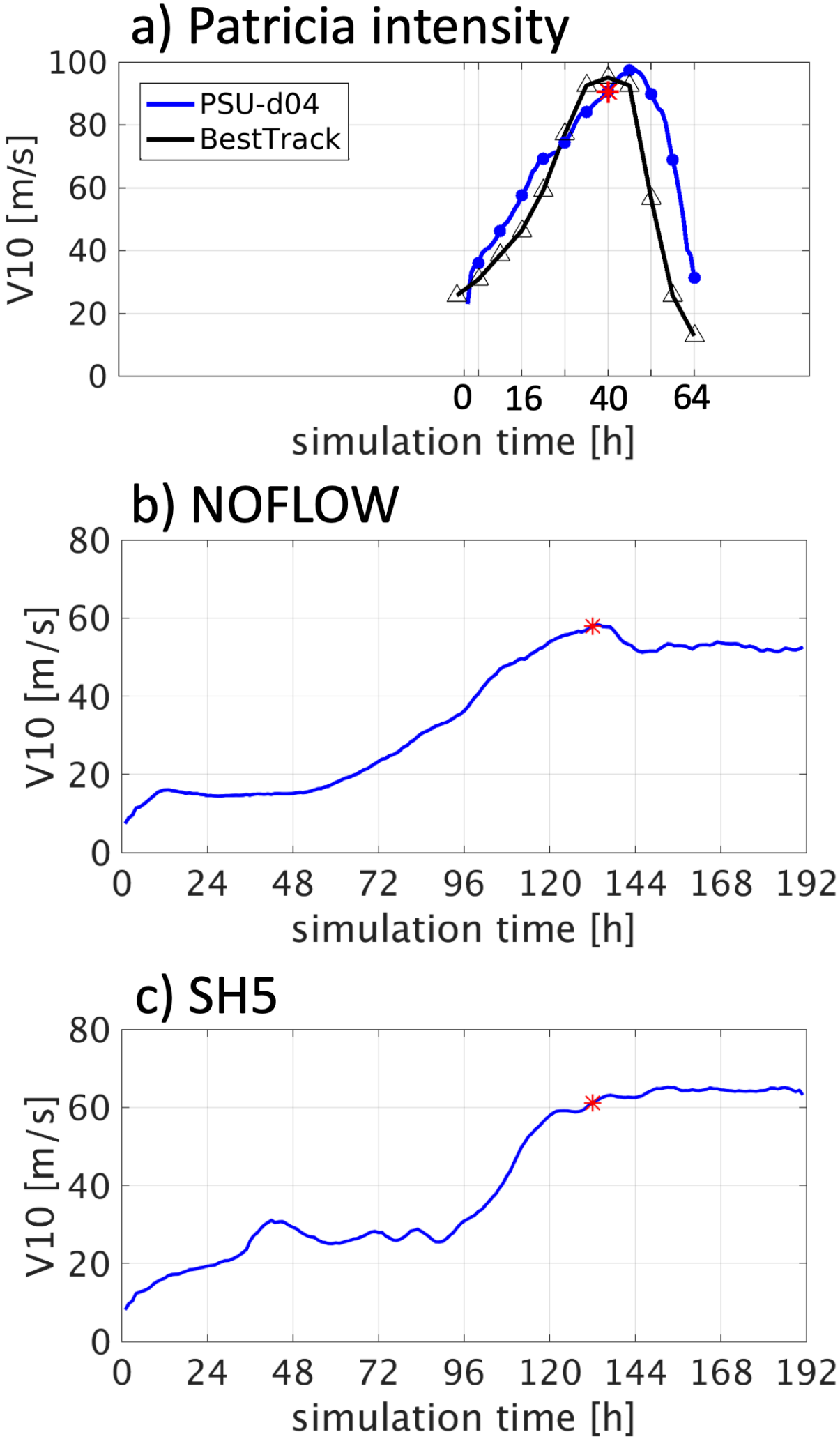

Figure 2



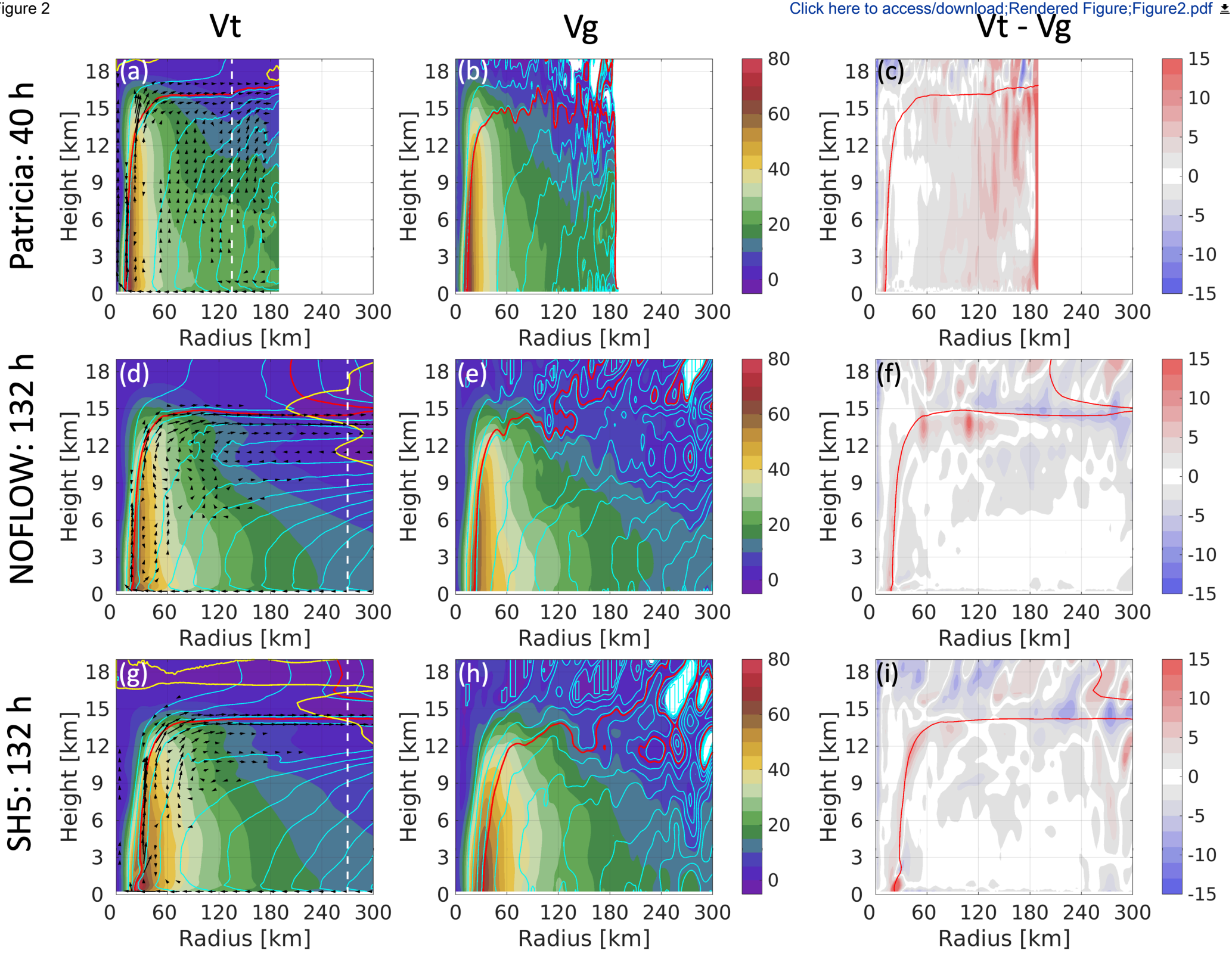

Figure 3



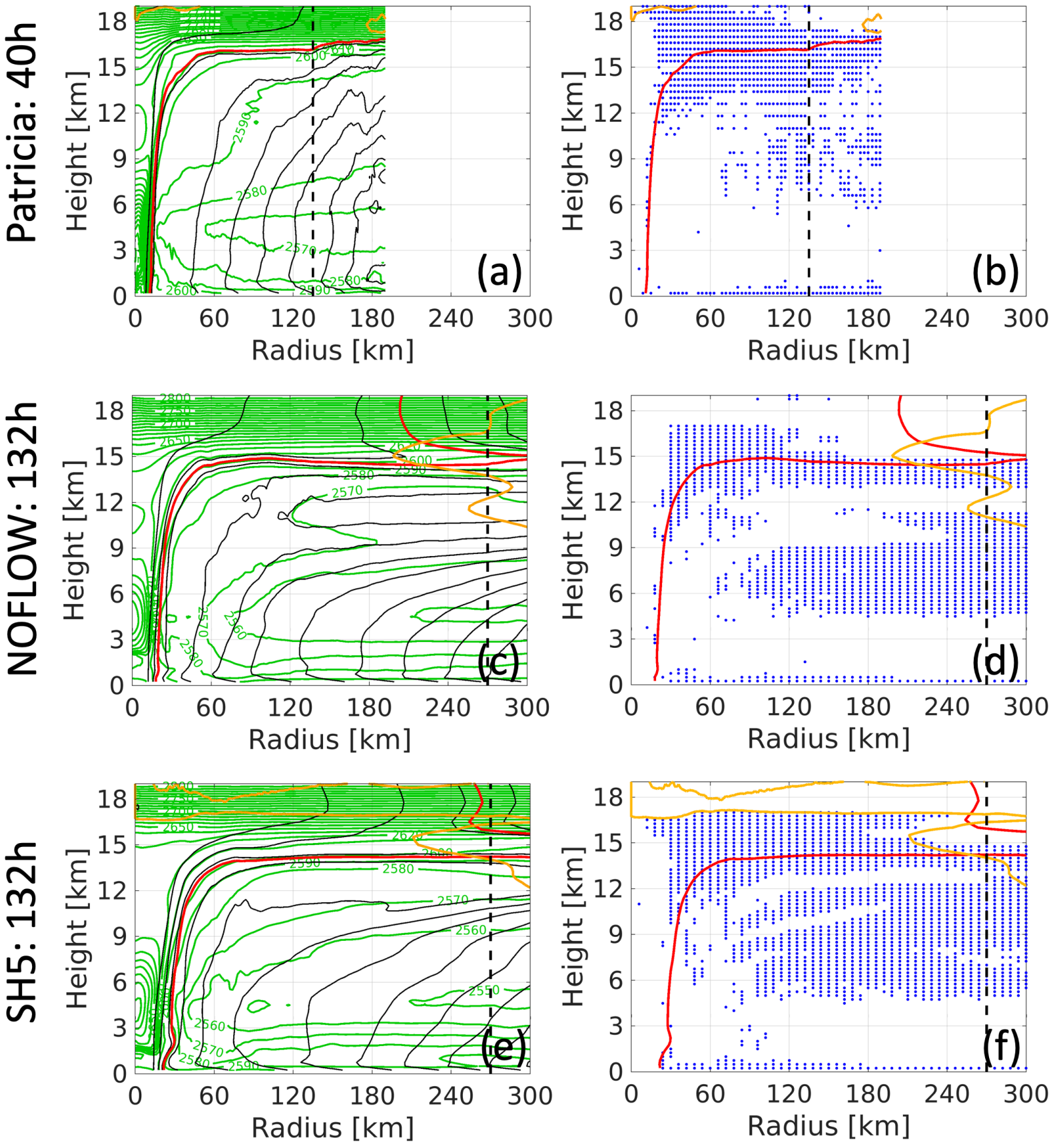

Figure 4



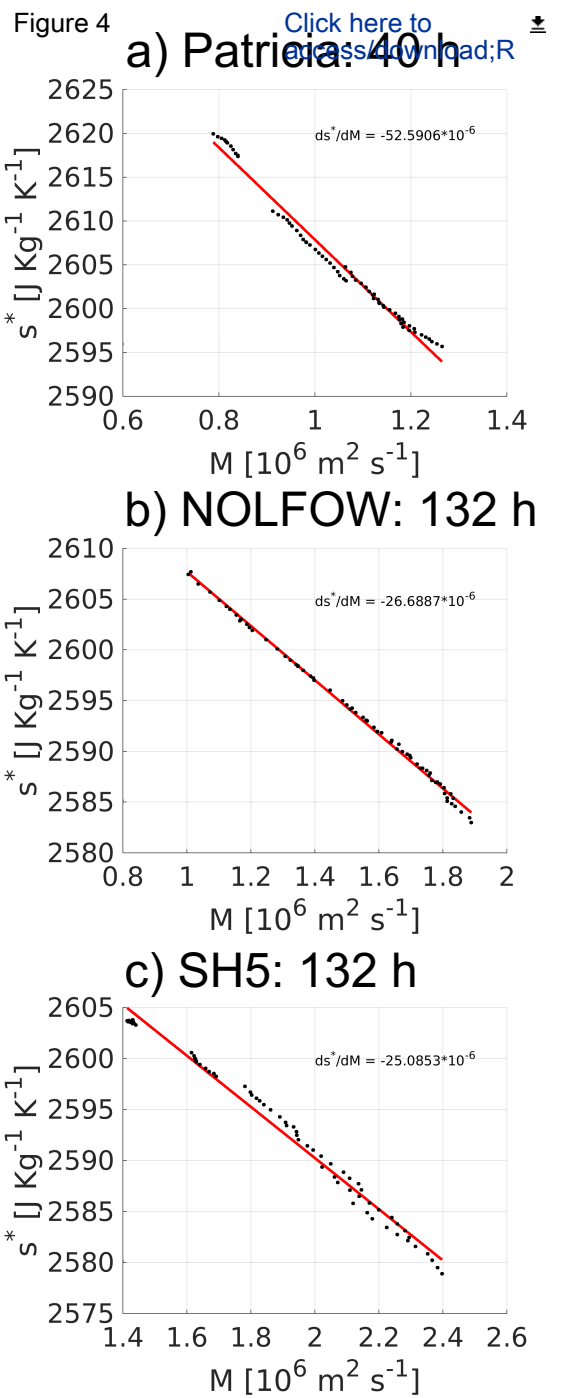

Figure 5



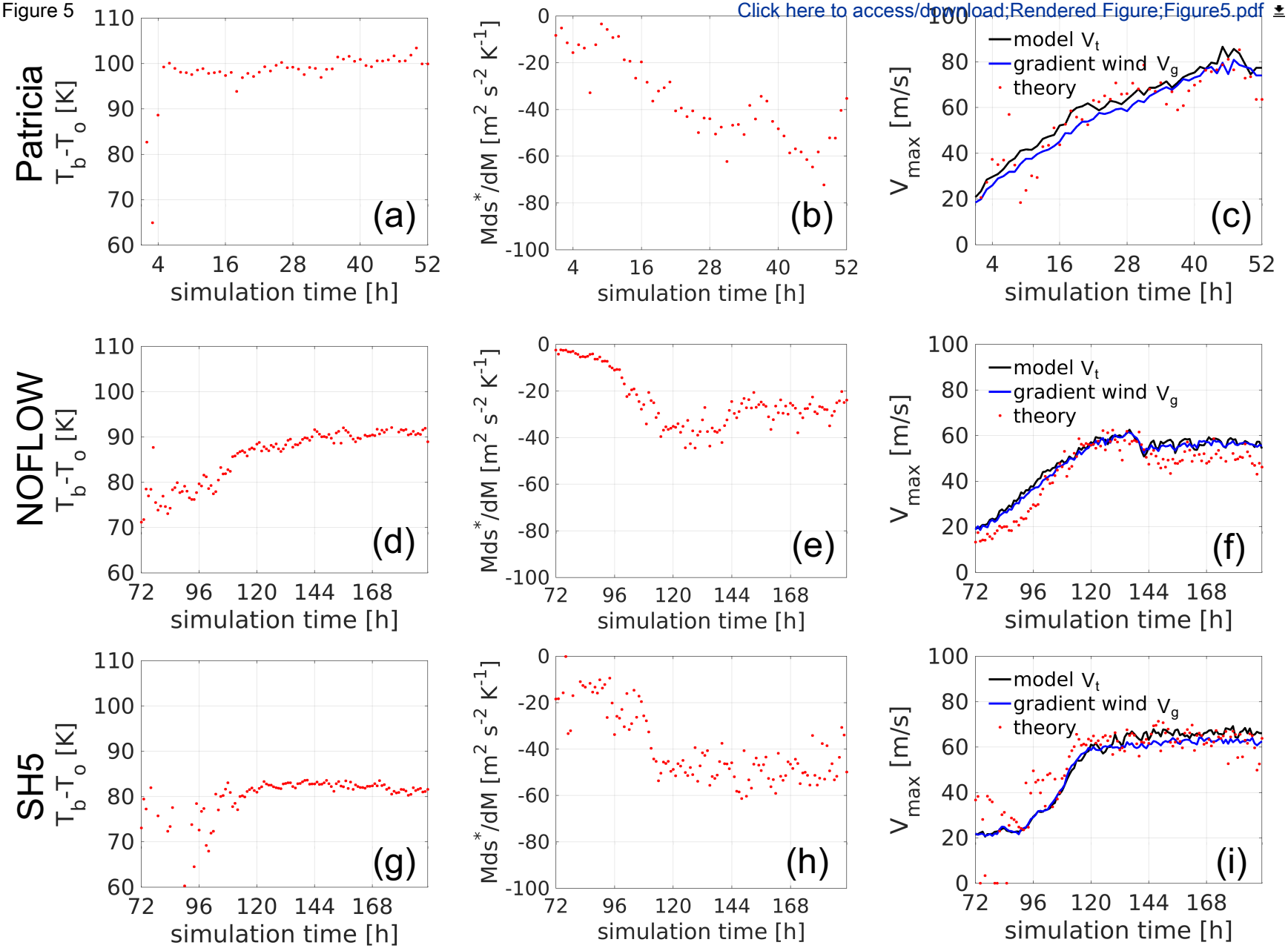

Figure 6

Click here to access/download;Rendered Figure;Figure6.pdf

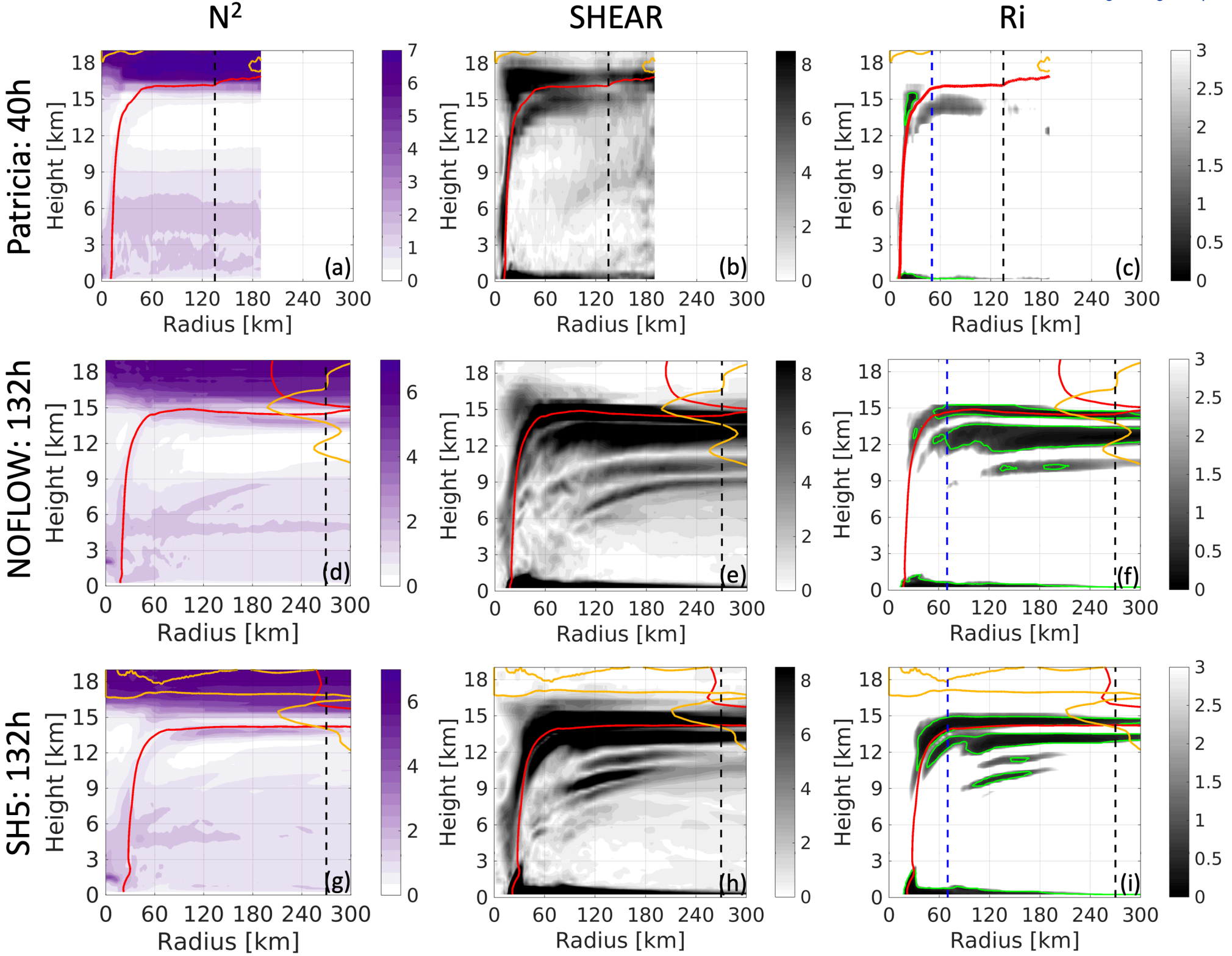

Figure 7



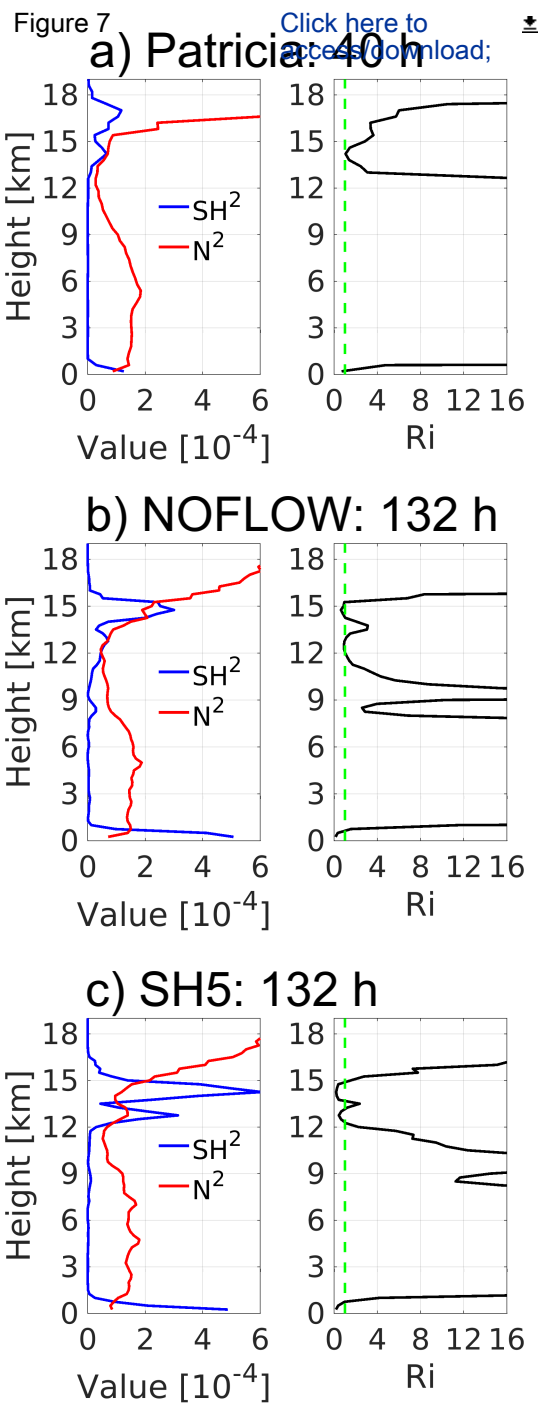

Figure 8

Click here to access/download;Rendered Figure;Figure8.pdf

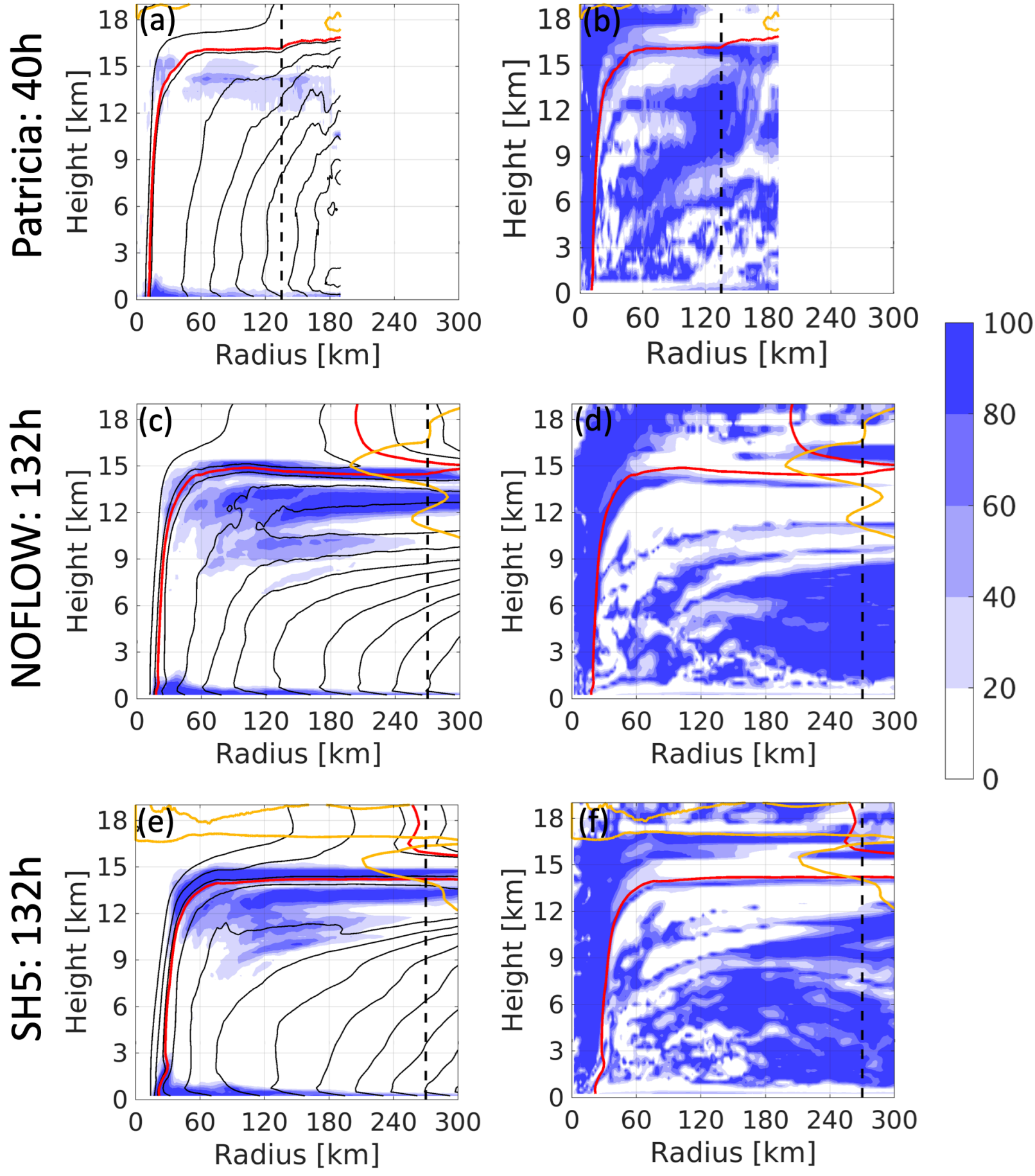

Figure 9



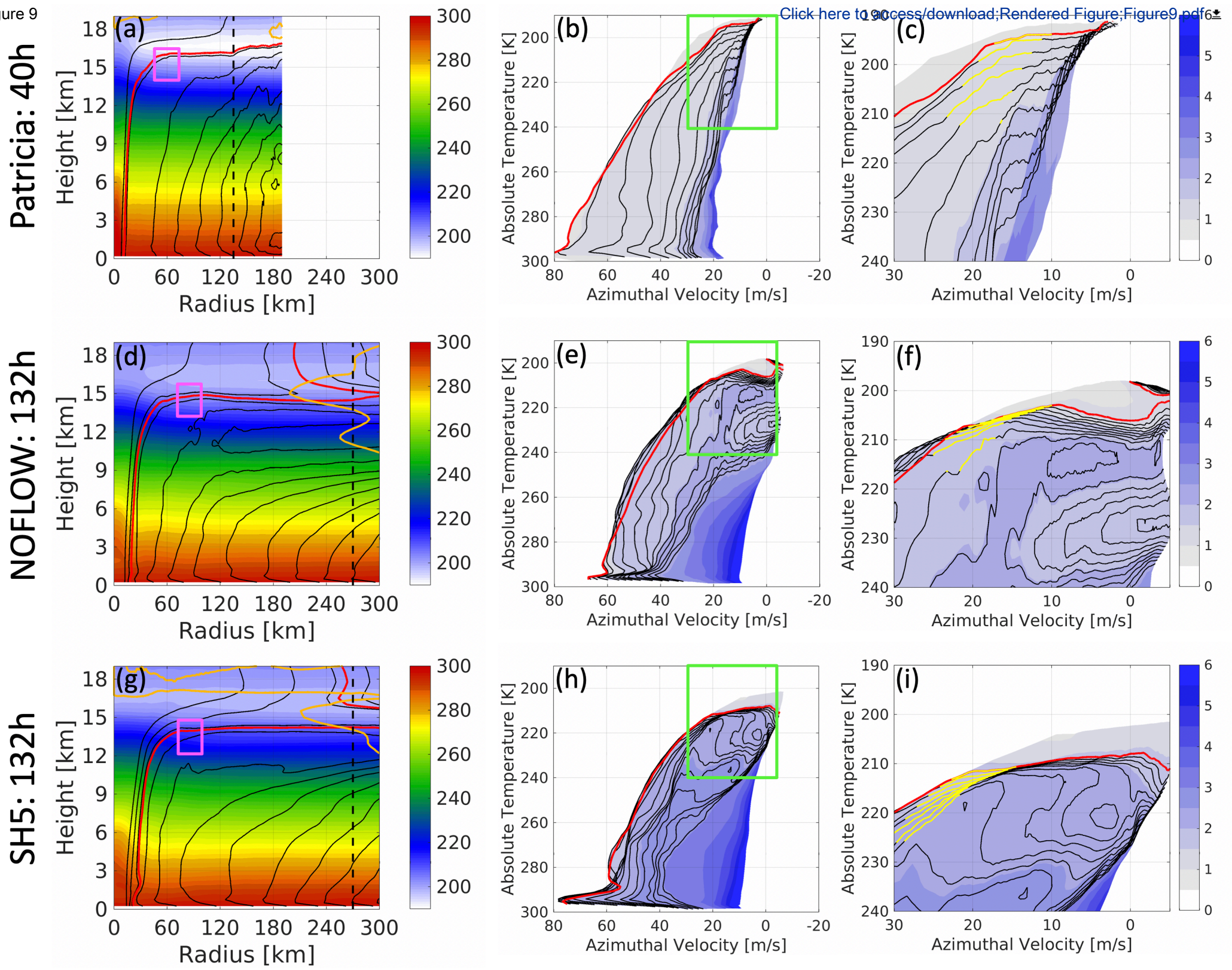

Figure 10